Biochimica et Biophysica Acta 1853 (2015) 2731–2744

Contents lists available at ScienceDirect

Biochimica et Biophysica Acta

journal homepage: www.elsevier.com/locate/bbamcr

# *Tfp1* is required for ion homeostasis, fluconazole resistance and *N*-Acetylglucosamine utilization in *Candida albicans*

Chang Jia [a], Kai Zhang [a], Qilin Yu [a], Bing Zhang [a], Chenpeng Xiao [a], Yijie Dong [a], Yulu Chen [a], Biao Zhang [b], Laijun Xing [a], Mingchun Li [a,*]

[a] Key Laboratory of Molecular Microbiology and Technology, Ministry of Education, Department of Microbiology, College of Life Sciences, Nankai University, Tianjin 300071, China
[b] Tianjin University of Traditional Chinese Medicine, Tianjin 300193, China

ARTICLE INFO

*Article history:*
Received 3 April 2015
Received in revised form 31 July 2015
Accepted 5 August 2015
Available online 7 August 2015

*Keywords:*
*Candida albicans*
V-ATPase
Tfp1
Ion homeostasis
Fluconazole
GlcNAc

ABSTRACT

The vacuolar-type $H^+$-ATPase (V-ATPase) is crucial for the maintenance of ion homeostasis. Dysregulation of ion homeostasis affects various aspects of cellular processes. However, the importance of V-ATPase in *Candida albicans* is not totally clear. In this study, we demonstrated the essential roles of V-ATPase through Tfp1, a putative V-ATPase subunit. Deletion of *TFP1* led to generation of an iron starvation signal and reduced total iron content, which was associated with mislocalization of Fet34p that was finally due to disorders in copper homeostasis. Furthermore, the *tfp1*Δ/Δ mutant exhibited weaker growth and lower aconitase activity on nonfermentable carbon sources, and iron or copper addition partially rescued the growth defect. In addition, the *tfp1*Δ/Δ mutant also showed elevated cytosolic calcium levels in normal or low calcium medium that were relevant to calcium release from vacuole. Kinetics of cytosolic calcium response to an alkaline pulse and *VCX1* (*VCX1* encodes a putative vacuolar $Ca^{2+}/H^+$ exchanger) overexpression assays indicated that the cytosolic calcium status was in relation to Vcx1 activity. Spot assay and concentration-kill curve demonstrated that the *tfp1*Δ/Δ mutant was hypersensitive to fluconazole, which was attributed to reduced ergosterol biosynthesis and *CDR1* efflux pump activity, and iron/calcium dysregulation. Interestingly, carbon source utilization tests found the *tfp1*Δ/Δ mutant was defective for growth on *N*-Acetylglucosamine (GlcNAc) plate, which was associated with ATP depletion due to the decreased ability to catabolize GlcNAc. Taken together, our study gives new insights into functions of Tfp1, and provides the potential to better exploit V-ATPase as an antifungal target.



## 1. Introduction

The organelle vacuole serves as the main ion pool, and has a central role in sequestering and storing metal ions. Vacuolar $H^+$-ATPases (V-ATPases) are ubiquitous proton pumps that couple ATP hydrolysis to proton translocation across the membranes of intracellular compartments, and, in some cases, the plasma membrane [1,2]. The proton gradient across the membrane plays an important role in regulating ion transport. Loss of V-ATPase activity compromises cellular pH homeostasis through indirectly affecting the plasma membrane proton pump (Pma1) [3], alkali cation/$H^+$ exchangers [4], and vacuolar buffering systems [4].

The critical role of V-ATPase in cation homeostasis was revealed in the response to diverse chemical agents that trigger cation stress [5]. These agents include membrane active compounds that trigger ion fluxes [6], cation chelating agents or environmental conditions that starve the fungi of essential cations such as $Ca^{2+}$ and $Fe^{2+}$ (EGTA, BPS, alkaline pH), and toxic levels of cations that exceed cellular homeostatic mechanism ($Zn^{2+}$, $Mn^{2+}$) [7]. Iron is an essential nutrient with limited bioavailability for most organisms. The ability of *Candida albicans* to acquire iron is deemed essential in pathogen–host interactions and has a profound influence on many cellular processes. The competition between pathogens and their hosts for iron serves as *C. albicans* to evolve various strategies to regulate iron acquisition, storage and utilization. In *Saccharomyces cerevisiae*, there is a high-affinity iron transport system which consists of a copper-containing iron oxidase, Fet3p, and a $Fe^{3+}$-specific iron transporter, Ftr1p [8]. Fet3p is required for Ftr1p to exit the endoplasmic reticulum (ER), and then the complex is transported to the Golgi to undergo glycosylation [9]. Subsequently, Fet3p is loaded with copper in a late Golgi or post-Golgi compartment. The mature protein complex was eventually moved onto the plasma membrane for iron uptake. Therefore, the proper function of Fet3p requires both normal copper homeostasis and vesicular traffic [10]. Interestingly, loading of Fet3p with copper requires the acidification of post-Golgi vesicular compartments, which is determined by

*Abbreviations:* V-ATPase, the vacuolar-type $H^+$-ATPase; YPG, YP + 2% glycerol; BPS, bathophenanthroline disulfonate; EGTA, ethylene glycol tetraacetic acid; GlcNAc, *N*-Acetylglucosamine.

* Corresponding author at: Department of Microbiology, College of Life Science, Nankai University, Tianjin 300071, China.
*E-mail address:* nklimingchun@163.com (M. Li).

http://dx.doi.org/10.1016/j.bbamcr.2015.08.005
0167-4889/

the vacuolar $H^+$-ATPase [10]. Any of these process defects results in the appearance of apoFet3p on the cell surface and an inability to grow on low iron medium. In *S. cerevisiae*, loss of vacuolar $H^+$-ATPase (V-ATPase) activity results in a striking induction of iron import and mobilization genes controlled by the transcription factor Aft1, which is characteristic of an iron deficiency signal [11]. However, the relationship between vacuolar $H^+$-ATPase and iron homeostasis in *C. albicans* remains to be elucidated.

Calcium, as a second messenger, is of vital importance to many physiological processes. Thus, the intracellular concentration of calcium is strictly controlled. In the budding yeast, cytosolic calcium concentration is typically maintained at low levels (sub-micromolar) by a calcium homeostasis system [12]. Stimulus-dependent opening of $Ca^{2+}$ channels in plasma membrane and/or internal compartments triggers a rapid increase in cytosolic calcium concentration in the cytosol, which is followed by efflux from cell or uptake back into internal stores to return cytosolic $Ca^{2+}$ to normal level. The pathogen *C. albicans* harbors putative $Ca^{2+}/H^+$ exchanger Vcx1, $Ca^{2+}$ pump Pmc1 [13] and $Ca^{2+}$ channel Yvc1 [14] in the vacuolar membrane, and $Ca^{2+}$ pump Pmr1 in the Golgi membrane [15], which may collaborate to maintain cytosolic calcium homeostasis. In *S. cerevisiae*, the $Ca^{2+}/H^+$ exchanger Vcx1, as a high capacity and low affinity vacuolar $Ca^{2+}$ transporter, could efficiently transport $Ca^{2+}$ at a high concentration burst of cytosolic $Ca^{2+}$ [16], which is dependent on the activity of V-ATPase [17]. $Ca^{2+}$-ATPase Pmc1 is a high affinity $Ca^{2+}$ transporter that can mediate transport in response to subtle changes in cytosolic $Ca^{2+}$. Yvc1 is responsible for $Ca^{2+}$ release from vacuole to cytosol. Pmr1 supplies the Golgi body with calcium and manganese. In addition, there is a high affinity calcium system (HACS) comprised of Mid1, Cch1 and Ecm7 in the plasma membrane [18]. All these transporters participate in maintaining cellular calcium homeostasis.

The azoles, particularly fluconazole, are the most widely used antifungals for the treatment of *C. albicans* [19]. The main mechanisms of azole resistance include a defective Erg3 function, overexpression or mutation of the target gene *ERG11*, overexpression of genes encoding membrane transport protein such as ABC (ATP binding cassette) transporters (e.g. *CDR1*) and/or the major facilitator superfamily (*MFS*) (e.g. *MDR1*) [20]. In addition, the elevated sensitivity to fluconazole is also related to dysregulation of iron [21] and/or calcium homeostasis [22]. A strain defective in iron uptake shows enhanced susceptibility to azole antifungal drugs in *Cryptococcus neoformans* [21]. Strains defective in the putative plasma membrane calcium channel (Cch1-Mid1) were modestly more susceptible to fluconazole and showed a significant loss of viability upon prolonged fluconazole exposure, suggesting that calcium signaling is required for survival of azole stress in *Candida glabrata* [22]. These findings suggest that, in the absence of iron and/or calcium signaling, fluconazole has a fungicidal rather than a fungistatic effect. In addition, it has been shown that ergosterol depletion following azole antifungals might compromise V-ATPase and the V-ATPase is a downstream target of azole drug [6]. However, whether reduced V-ATPase activity has an effect on ergosterol biosynthesis following fluconazole treatment remains largely unknown.

*N*-Acetylglucosamine (GlcNAc) is an important carbon source for many pathogens and can also act as a signaling molecule. In *C. albicans*, multiple enzymes are required for the GlcNAc catabolism, including Ngt1 (a transporter that takes up GlcNAc), Hxk1 (a kinase that converts GlcNAc to GlcNAc-6-phosphate), Dac1 (a deacetylase that converts GlcNAc-6-phosphate to glucosamine-6-phosphate) and Nag1 (a deaminase that converts glucosamine-6-phosphate to glucose-6-phosphate). Ngt1 is the first identified eukaryotic GlcNAc transporter, which is a useful tool for studying the roles of GlcNAc in other organisms [23]. In *Streptomyces coelicolor*, GlcNAc could inhibit siderophore production via DasR, the GlcNAc utilization regulator, thus limiting iron uptake and utilization, suggesting there is a relationship between nutrient and iron [24]. Previous studies show that GlcNAc could inhibit growth of some mutants due to the depletion of ATP [25] or toxic GlcNAc derivatives. However, there is no report about the relation between V-ATPase and GlcNAc.

Therefore, we tested a series of functions of Tfp1, a putative V-ATPase subunit. In this study, we found that deletion of *TFP1* generates an iron deprivation signal and leads to elevated cytosolic calcium levels, which first reveals the intimate correlation between vacuolar $H^+$-ATPase and iron/calcium homeostasis in *C. albicans*. Furthermore, the *tfp1*Δ/Δ cells are hypersensitive to antifungal drugs due to defective ergosterol biosynthesis, reduced *CDR1* efflux pump activity and dysregulation of iron/calcium homeostasis, which for the first time demonstrate that the antifungal activity of fluconazole is involved in V-ATPase activity in *C. albicans*. In addition, the *tfp1*Δ/Δ mutant is unable to utilize GlcNAc as the sole carbon source owing to decreased mRNA levels of GlcNAc catabolic genes, which might be related to the role of V-ATPase in non-ionic homeostasis. Taken together, our results highlight the pleiotropic effects that occur in cells with deletion of *TFP1* and validate Tfp1 as a potential drug target.

## 2. Materials and methods

### 2.1. Strains and media

The *C. albicans* strains used in the present study were listed in Table 1. The *C. albicans* cells were routinely grown at 30 °C in YPD medium (2% glucose, 2% peptone, 1% yeast extract) supplemented with 80 μg/ml uridine, or synthetic drop-out medium (0.67% yeast nitrogen base (YNB) without amino acid, 2% glucose, 0.2% complete mixture lacking specific amino acid) for selection of specific transformants. For spot growth assay, YPD medium containing fluconazole, terbinafine was achieved at the indicated concentrations, respectively. Bathophenanthroline disulfonate (BPS, Sigma) was added to achieve iron-limited conditions. For nonfermentable carbon source utilization tests, YP medium (1% yeast extract, 2% peptone) was supplemented with 2% acetate, 2% ethanol, 2% glycerol, and 1% ethanol plus 1% glycerol, respectively. For test of different substrates as sole carbon sources, YNB with complete amino acid mix was supplemented with 2% glucose, 2% fructose, 2% galactose, 2% sucrose, 2% maltose, 2% GlcNAc, 1% galactose plus 1% GlcNAc, respectively.

### 2.2. Strain constructions

*C. albicans* mutant strains used in this study were constructed by PCR-mediated homologous recombination in *C. albicans* strain SN76 as described previously [26].

A Fet34-GFP reporter gene was introduced into the indicated wild type and *tfp1*Δ/Δ mutant strains by PCR-mediated homologous recombination of GFP sequences to replace the open reading frame of one copy of Fet34p using previously described methods [27]. Primers FET34-GFP-1 and FET34-GFP-2 containing ~60 bp of sequence homologous to the 5′ and 3′ ends of the *FET34* open reading frame were used to amplify a cassette from pGFP-URA3 containing a GFP fragment and a URA3 selectable marker. Following transformation into *C. albicans*, the $URA^+$ colonies were confirmed by PCR to carry the FET34-GFP reporter gene.

The strains producing Fet34-HA fusion proteins were constructed by PCR-mediated homologous recombination as above described. Briefly, the Fet34::3×HA-URA3 cassette containing the flanking homology was amplified from the pFA-HA-URA3 template. Then, the cassette was transformed into SN76 and the *tfp1*Δ/Δ strains to generate correct recombinants.

### 2.3. RNA isolation and quantitative real-time PCR

For RNA preparation, cells were grown under appropriate media to log phase. Then, cultures were harvested and cell pellets were frozen in liquid nitrogen. Total RNA was extracted by the phenol/chloroform

**Table 1**
Strains and plasmids used in this study.

| Strain/plasmid | Genotype and description | Source |
|---|---|---|
| Strains | | |
| SN76 | *ura3Δ::λimm434/ura3Δ::λimm434 his1::his G/his1::his G arg4::his G /arg4::his G* | [26] |
| *tfp1Δ/Δ* | *ura3Δ::λimm434/ura3Δ::λimm434 his1::his G/his1::his G arg4::his G/arg4::his G tfp1::CdARG4/tfp1::CaHIS1* | [7] |
| *tfp1Δ/Δ + TFP1* | *ura3Δ::λimm434/ura3Δ::λimm434 his1::his G/his1::his G arg4::his G/arg4::his G tfp1::CdARG4/tfp1::CaHIS1 ADE2::pBES116-TFP1-URA3* | [7] |
| SN76-Fet34-HA | *ura3Δ::λimm434/ura3Δ::λimm434 his1::his G/his1::his G arg4::his G/arg4::his G FET34/FET34-3×HA::URA3* | This study |
| *tfp1Δ/Δ-Fet34-HA* | *ura3Δ::λimm434/ura3Δ::λimm434 his1::his G/his1::his G arg4::his G/arg4::his G tfp1::CdARG4/tfp1::CaHIS1 FET34/FET34-3×HA::URA3* | This study |
| SN76-Fet34-GFP | *ura3Δ::λimm434/ura3Δ::λimm434 his1::his G/his1::his G arg4::his G/arg4::his G FET34/FET34-GFP::URA3* | This study |
| *tfp1Δ/Δ-Fet34-GFP* | *ura3Δ::λimm434/ura3Δ::λimm434 his1::his G/his1::his G arg4::his G/arg4::his G tfp1::CdARG4/tfp1::CaHIS1 FET34/FET34-GFP::URA3* | This study |
| *vcx1Δ/Δ* | *ura3Δ::λimm434/ura3Δ::λimm434 his1::his G/his1::his G arg4::his G/arg4::his G vcx1::CdARG4/vcx1::CaHIS1* | This study |
| SN76 + $VCX1_{ACT1p}$ | *ura3Δ::λimm434/ura3Δ::λimm434 his1::his G/his1::his G arg4::his G /arg4::his G pAU34M-ACT1-VCX1::URA3* | This study |
| *tfp1Δ/Δ* + $VCX1_{ACT1p}$ | *ura3Δ::λimm434/ura3Δ::λimm434 his1::his G/his1::his G arg4::his G/arg4::his G tfp1::CdARG4/tfp1::CaHIS1 pAU34M-ACT1-VCX1::URA3* | This study |
| *tfp1Δ/Δpmc1Δ/Δ* | *ura3Δ::λimm434/ura3Δ::λimm434 his1::his G/his1::his G arg4::his G/arg4::his G tfp1::CdARG4/tfp1::CaHIS1 pmc1::dpl200/pmc1::URA3-dpl200* | This study |
| Plasmids | | |
| pSN69 | Containing *ARG4* marker, $Kan^r$ | [26] |
| pSN52 | Containing *HIS1* marker, $Kan^r$ | [26] |
| pBES116 | *ADE2-URA3-ADE2*, *Asc*I fragment in pBluescript II KS (+) | G. Fink |
| pBES116-TFP1 | 3.2 kb full-length *C. albicans TFP1* in pBES116 | [7] |
| pAU34M-GFP | $Ap^R$ $P_{ACT1}$-*GFP-URA3* | [14] |
| pAU34M-ACT1-VCX1 | $Ap^R$ $P_{ACT1}$-*VCX1-URA3* | This study |
| pFA-HA-URA3 | Containing a 1.8kb HA-URA3 cassette | [7] |
| pGFP-URA3 | Containing a GFP fragment and URA3 sequence | [71] |

method as previously described [28]. The overall quality of RNA was analyzed by agarose gel electrophoresis. Quantitative real-time PCR was performed in triplicate and repeated in three independent experiments with Mastercycler ep realplex system. The primers used were listed in Table 2. The SYBR Green qPCR SuperMix (TransGen Biotech) was used for the real-time PCR analysis, and the *ACT1* transcripts were used as an endogenous control for the quantitative PCR. The relative changes in gene expression were determined by the $2^{-\triangle\triangle CT}$ method.

For GlcNAc catabolic gene expression, cells were grown overnight to log phase, washed, and then incubated in synthetic medium containing 2% GlcNAc for 6 h, and the cells were harvested and frozen in liquid nitrogen. The RNA extraction and quantitative real-time PCR were carried out as described above.

### 2.4. Cellular iron content determination, iron uptake and ferric reductase assay

Cellular iron content was determined according to the bathophenanthroline disulfonate (BPS)-based colorimetric methods as described previously [29]. Overnight cultures were re-cultivated in YPD or YPG (YP + 2% glycerol) medium to log-phase. The cells were harvested, washed three times and re-suspended in 500 μl of 3% nitric acid, and boiled for 2 h to digest the cells completely. 400 μl of cell supernatant was then mixed with 160 μl of 38 mg/ml sodium ascorbate, 320 μl of 1.7 mg/ml BPS, and 126 μl of 4 M ammonium acetate. After 10-min incubation at room temperature, the $OD_{535}$ of the BPS–Fe complex was determined by the Ultrospec 1000 UV–Visible spectrophotometer. $OD_{680}$ was also recorded as the nonspecific absorbance. Experiments were performed in triplicate. And the iron content was calculated as the following formula: ($OD_{535}$ − $OD_{680}$) / cell number, and displayed in arbitrary units (A.U.). The data were present as means ± standard deviation (SD) from a single experiment representative of three independent experiments.

The iron uptake assay was evaluated by measuring the increase in intracellular iron levels after 3 h of iron uptake in fresh YPD medium. Mid-exponential phase strains were pre-grown in YPD medium for 24 h. These stationary-phase cells were harvested, and re-suspended in fresh YPD medium at an optical density of 2.0. After 3 h incubation, cells were harvested immediately, and washed with deionized water for three times. Intracellular iron levels at the indicated time point were measured by BPS-based colorimetric methods as described above. Iron uptake activity was determined by the increase in intracellular iron content, and presented as the increased iron content per hour. The experiments were repeated independently three times with similar results.

The ferric reductase assay was conducted according to the description previously [30] with a little modification. Briefly, cells were harvested and washed three times with Assay buffer (50 mM citrate buffer, 5% glucose; pH 6.5), and incubated in Assay buffer at 37 °C in the presence of 1 mM BPS and 1 mM ferric trichloride. After 15 min, cells were removed by centrifugation, and the optical density of the supernatant was measured at 520 nm. The activity was calculated as the following formula: A520 × 4/22,140 × cell number, and displayed in nmol Fe(II)/million cells/h. Experiments were conducted three times. Data shown are representative of three independent experiments.

### 2.5. Metal analysis by ICP-MS

The overnight cultures of wild-type strain SN76 and the *tfp1Δ/Δ* mutant were refreshed in YPD medium for 18 h, collected by centrifugation, and washed twice with 1 mM EDTA and three times with deionized water. Cell pellets were weighed, and digested in 500 μl of 30% nitric acid ($HNO_3$) at 100 °C for 2 h. After digestion, the samples were diluted to 5 ml with deionized water and analyzed using a Perkin Elmer ICP-MS to determine the metal content. The experiments were repeated three times. The data were expressed as μg of metal/g fungal cells.

### 2.6. Western blotting and aconitase activity assay

Overnight cultures of the strains producing Fet34-HA protein were re-cultivated to log phase in YPD medium. Protein extracts were prepared by breakage with glass beads according to previously described protocol [32]. Lysates were analyzed by SDS-PAGE, and immunoblotted with mouse anti-HA high-affinity antibodies (Sigma) for HA-tagged proteins. And anti-alpha tubulin antibody (Novus Biologicals) was used as a loading control.

Aconitase activity assay is based on the formation of isocitrate by the iron–sulfur protein aconitase, which is used by isocitrate dehydrogenase (IDH) for the reduction of NADP [31]. The aconitase-catalyzed isocitrate formation from *cis*-aconitate is coupled with isocitrate dehydrogenase and NADP. Briefly, cells cultivated in YPG were harvested and the cell extracts (>50 μg protein) were added to the sample cuvette which contained 950 μl of aconitase buffer (100 mM triethanolamine, 1.5 mM $Mg^{2+}$, 0.1% Triton X-100; pH 8.0), 200 μM *cis*-aconitase,

**Table 2**
List of primers used in this study.

| Primer | Sequence (5′–3′) |
|---|---|
| ACT1-5RT | GGTAGACCAAGACATCAAGG |
| ACT1-3RT | CCGTGTTCAATTGGGTATCT |
| SEF1-5RT | ATCCCCTACACCAACCAAC |
| SEF1-3RT | CATGAAGTCACTGGCCTATG |
| HAP43-5RT | GATCACCACCTTCATCATCTG |
| HAP43-3RT | GACGCTGGAGTATCAACACT |
| FTH1-5RT | TGATTTGTGGACCGTAGCTG A |
| FTH1-3RT | GCCAACACAGCAGCATTTACA |
| FRE10-5RT | ATTATTTGCTGCCATCACGTTG |
| FRE10-3RT | GCTTTATCAGTGGTTTCGTTGA |
| FTR1-5RT | CTTCATCGTTTTCAGAGAAT |
| FTR1-3RT | CAACCAATAATAAGACAGAC |
| ARN1-5RT | CTGGTGCTGTGTTGTTCC |
| ARN1-3RT | AGCCCACATCCCGATACC |
| AFT2-5RT | GATGATATCAAGCCATGGC |
| AFT2-3RT | CCTCACACTATAGTTAGCTC |
| ISU1-5RT | TCCAAGATTAGCTATTCCAAC |
| ISU1-3RT | CCCGTTTCTTCATCAACCTG |
| CFL1-5RT | AAGTGGTAAAGGCAACAGCG |
| CFL1-3RT | ACCAAGTAACCCTGAACCGT |
| CTR1-5RT | GATTCAGCCACATCAATGGT |
| CTR1-3RT | CATACCTTCCATAGCCATAC |
| CUP2-5RT | GTATCAGAGGTCATCGTGTC |
| CUP2-3RT | CTTATGACAAGCACATGAAGG |
| CCC2-5RT | TGTCACGGTGGTTTTGGAAG |
| CCC2-3RT | AGAGTAAGTTCTTGATGATCG |
| ERG1-5RT | GTACGTGGGGCTGCATTTC |
| ERG1-3RT | CACTGGGTTGTTTTGTTTGC |
| ERG3-5RT | TGCCACTACTGCCATTCCAG |
| ERG3-3RT | GGCCAGTGTAACCATCTATG |
| ERG11-5RT | CTGAGAAGAGAACGTGGTGA |
| ERG11-3RT | GAAGTAGAAGCAGAAGTATGTTG |
| CDR1-5RT | TGAATACCACGGGTTTGATG |
| CDR1-3RT | TCATGTTCATATGGATTGACC |
| MDR1-5RT | GCCGATTACAAACCAACTCT |
| MDR1-3RT | ATCATCATCACCATCCCAAG |
| CCH1-5RT | GAAACCAATGCAACACCATTC |
| CCH1-3RT | GCACCAATATCTTCTTAACTCG |
| MID1-5RT | TAACCGAGACCACCACCAC |
| MID1-3RT | CCCCGTCACTATTAATGCACTA |
| PMC1-5RT | CCCGTTGCTAAAGCCATGAA |
| PMC1-3RT | GAAATCCCTTCTGCCAAATC |
| VCX1-5RT | GCTGGTGGGATTACAAGAGT |
| VCX1-3RT | AACGATCAACAAGACAACGG |
| PMR1-5RT | CAGTGTTTGAAATGATGAGCGAC |
| PMR1-3RT | CTTCAGGAATAGCAGCAACC |
| YVC1-5RT | TTAACGGAGTGGATGCTACC |
| YVC1-3RT | GGAGTTTTGATTCTGGCAGG |
| RTA2-5RT | TCATCATGGCAGGTGTATAC |
| RTA2-3RT | CCCGACTGAACTATCTTTATG |
| HKX1-5RT | CTGTCGTTGAAAGAGAATTCC |
| HKX1-3RT | CACAACTATAGTTATCCTCTC |
| DAC1-5RT | CCCTGAGTTGGTTAGTGAGG |
| DAC1-3RT | ACAGTAGGACACGTAGCAGT |
| NAG1-5RT | TTGCCAAAATCAACTCCACC |
| NAG1-3RT | CCAATCCCAAATACTCGTCC |
| FET34-HAF | GAACAAAGCATTACTGAGCAGGCTGCAACTGGTTCCTCTT |
| | CTAGCCCTTCAAACAAA |
| | CCCGGGTACCCATACGATGTTC |
| FET34-HAR | AGAATGTTGTTTCAATGTATAATCCATCAAAGAGAGTTACTT |
| | CACTGGGTCAATCAAA |
| | CATACGACTCACTATAGGGAG |
| FET34-GFP-1 | GAACAAAGCATTACTGAGCAGGCTGC |
| | AACTGGTTCCTCTTCTAGCCCTTCAAACAAA |
| | GGTGGTGGTTCTAAAGGTGAAGAATTATT |
| FET34-GFP-2 | TTCTTTGACTGTTATTCAACAACACCACTCTCTCGCCATATA |
| | AAAAAATTAACCAATTT |
| | CCTAGAAGGACCACCTTTGATTG |
| VCX1 primer1 | AGTCGTTTCTTTGTGGTTGT |
| VCX1 primer3 | CACGGCGCGCCTAGCAGCGGCTCTGTTGGTTTGTTTTATTTG |
| VCX1 primer4 | GTCAGCGGCCGCATCCCTGCTCATGATGATAAGAAAGAGG |
| VCX1 primer6 | AGACCTGCTTCATCTCACTT |
| Universal primer2 | CCGCTGCTAGGCGCGCCGTGACCAGTGTGATGGATATCTGC |
| Universal primer5 | GCAGGGATGCGGCCGCTGACAGCTCGGATCCACTAGTAACG |

1.3 mM $NADP^+$ and 400 μU IDH. After thoroughly mixing and 2-min incubation at room temperature, the increase of absorbance at 340 nm was determined every minute in double-beam spectrophotometer for 10–15 min. Aconitase activity was calculated using the absorption coefficient of 6220 $M^{-1}$ $cm^{-1}$, and expressed as nmol of *cis*-aconitase converted/min/mg protein. These experiments were performed at least three times independently. Data from one representative experiment are presented as means ± SD.

### 2.7. p-Phenylenediamine (PPD) oxidase assays

Plasma membrane extracts were obtained from the *tfp1*Δ/Δ mutant with or without $CuCl_2$ treatment using a method described by Marvin et al. [36]. Then the extracted plasma membrane was used to assay PPD oxidase activity as follows. 25 μg of the cell membrane protein fraction was resuspended in 600 μl assay buffer (100 mM sodium acetate pH 5.7, 0.06% Triton X-100, 0.05% PPD) and incubated at 30 °C for 1 h. Color development was followed in a spectrophotometer at 530 nm at 30 min intervals for a total of 2 h. Oxidation rates were calculated after subtracting the rate of a blank sample that contained assay buffer with no added protein. Experiments were repeated at least three times.

### 2.8. Drug susceptibility tests

For drug susceptibility analysis, overnight cultures were resuspended in YPD medium supplemented with 80 μg/ml uridine and grown to mid-log phase at 30 °C. Cultures were adjusted to an optical density of 0.2. A series of 10-fold dilutions were prepared in sterile distilled water. 3 μl of each dilution was spotted onto solid YPD medium with fluconazole, terbinafine, or SDS at the indicated concentrations. In addition, tolerance to fluconazole was assayed in liquid YPD medium with various concentrations of fluconazole as indicated. 100 μl of cells with a starting $OD_{600}$ of 0.1 in YPD medium was added to a 96-well plate. Then different concentrations of fluconazole were supplemented. Every treatment was conducted in triplicate and repeated in three independent experiments. Data from one representative experiment are presented as means ± SD.

### 2.9. Efflux of R6G

The efflux measurement of R6G was conducted according to the description by Thomas [33] with a small modification. Overnight cultures of each strain were resuspended in 100 ml YPD medium with a starting $OD_{600}$ of 0.5, and allowed to grow for 6 h. The cells were pelleted, washed twice with PBS buffer (pH 7.0), and resuspended in PBS to 2% cell suspension. R6G was added at a final concentration of 10 μM. Cell suspensions were incubated at 30 °C with shaking (200 rpm) for 3 h under glucose starvation conditions. The de-energized cells were then washed and resuspended again in PBS at a 2% cell suspension. At 10-min intervals, a portion (1 ml) of the cells was removed and centrifuged at 9000 ×*g* for 2 min, and the absorption of the supernatants was measured at 527 nm. At 10 min, 2% glucose was added to PBS to observe energy-dependent efflux activity. Experiments were carried out at least times, and data were shown from one representative experiment.

### 2.10. Cytosolic calcium level measurement

#### 2.10.1. Cytosolic calcium levels

Overnight cultures of the strains were refreshed in YPD medium and incubated at 30 °C for 4 h. Then the cells were centrifuged, washed three times with a Hank's balanced salt solution (HBSS) buffer (pH 7.2) and treated with fluo-3/AM (Sigma) at 37 °C for 50 min. After that, the pellets were collected, and washed three times, then measured using an excitation wavelength of 488 nm and an emission wavelength of 520 nm in a fluorescence plate reader (Enspire).

*2.10.2. Cytosolic calcium fluctuation*

Overnight cultures of SN76, *tfp1*Δ/Δ mutant, and *vcx1*Δ/Δ mutant were introduced into fresh YPD medium and incubated for 4 h. The cells were harvested, washed three times, and treated with fluo-3/AM at 37 °C for 50 min. After that, the pellets were harvested and washed three times. Calcium flux measurements were performed by flow cytometry, using a BD FACSCalibur flow cytometer (BD). The baseline ratio was acquired before the addition of KOH solution. Data were analyzed off-line using the WINMDI 2.9.

*2.11. ATP level determination*

Overnight cultures of the strains were harvested, washed, and then incubated in synthetic medium containing 2% GlcNAc for 6 h. The cells were harvested, and protein extracts were prepared by liquid nitrogen extraction. The cellular ATP levels were measured using ATP Assay Kit (Nanjing Jiancheng), according to the protocol. Experiments were conducted at least three times. And the data were shown as means ± SD.

## 3. Results

*3.1. Deletion of TFP1 triggers iron starvation signal*

Iron homeostasis is critical in cells since iron is an essential nutrient required for the growth and metabolism of *C. albicans* [34]. Previous study found that loss of V-ATPase activity in yeast generates an iron deprivation signal [11]. To investigate the effect of *TFP1* disruption on iron homeostasis in *C. albicans*, we determined the transcript expression of iron uptake-related genes. The results showed that deletion of *TFP1* led to up-regulation of iron import and mobilization genes (Fig. 1A), suggesting that the *tfp1*Δ/Δ mutant was starved of iron. In order to directly assess the iron status of *tfp1*Δ/Δ mutant, total cellular iron content was measured according to the bathophenanthroline disulfonate (BPS)-based colorimetric methods. As expected, the *tfp1*Δ/Δ mutant had significantly low total iron levels and iron uptake capacity in comparison with the wild-type strain (Fig. 1B, C). Therefore, it was anticipated that the high-affinity iron uptake system in the *tfp1*Δ/Δ mutant may be defective. To confirm this hypothesis, the activity of ferric reductases of high affinity iron acquisition system was measured. The results showed the activity of ferric reductases was significantly increased in the *tfp1*Δ/Δ mutant compared with the wild-type strain (Fig. 1D). One possibility is that the assembly of complexes of multicopper ferroxidase and high-affinity iron permease was presumed to be of imbalance. In *C. albicans*, Fet34p is assumed to be the major multicopper ferroxidase with a predicated role in high-affinity iron uptake [35]. The post-translational modification and proper localization of Fet34p are necessary for normal function [35]. Therefore, the protein expression and glycosylation of Fet34p were analyzed. Western blotting assay showed that there was no significant difference in protein expression of Fet34p between the *tfp1*Δ/Δ mutant and wild-type strain, and the Fet34p was normally glycosylated in both strains (Fig. 1E). However, the localization observation of Fet34p exhibited that a majority of Fet34-GFP fusion protein was shown on the cell surface of wild-type strain SN76 (Fig. 1F, upper). However, in the *tfp1*Δ/Δ mutant Fet34p was dispersed in the cytosol (Fig. 1F, bottom). In *S. cerevisiae*, copper is required for the activation of Fet3p oxidase in the high affinity iron uptake system [36]. And the loading of copper onto Fet3p takes place in post-Golgi vesicles, which needs both normal copper homeostasis and vesicular traffic [10]. Therefore, we speculated that the reduced iron uptake and growth defect on low iron in the *tfp1*Δ/Δ mutant should be associated with disorders in copper homeostasis [37]. To substantiate the speculation, we measured the total copper levels in both wild-type strain SN76 and the *tfp1*Δ/Δ mutant. The ICP assay showed that the *tfp1*Δ/Δ mutant exhibited elevated copper content (Fig. 1G). Further phenotype observation found that the *tfp1*Δ/Δ mutant was sensitive to both low and high copper (Fig. 1H). These results suggest that disruption of *TFP1* indeed

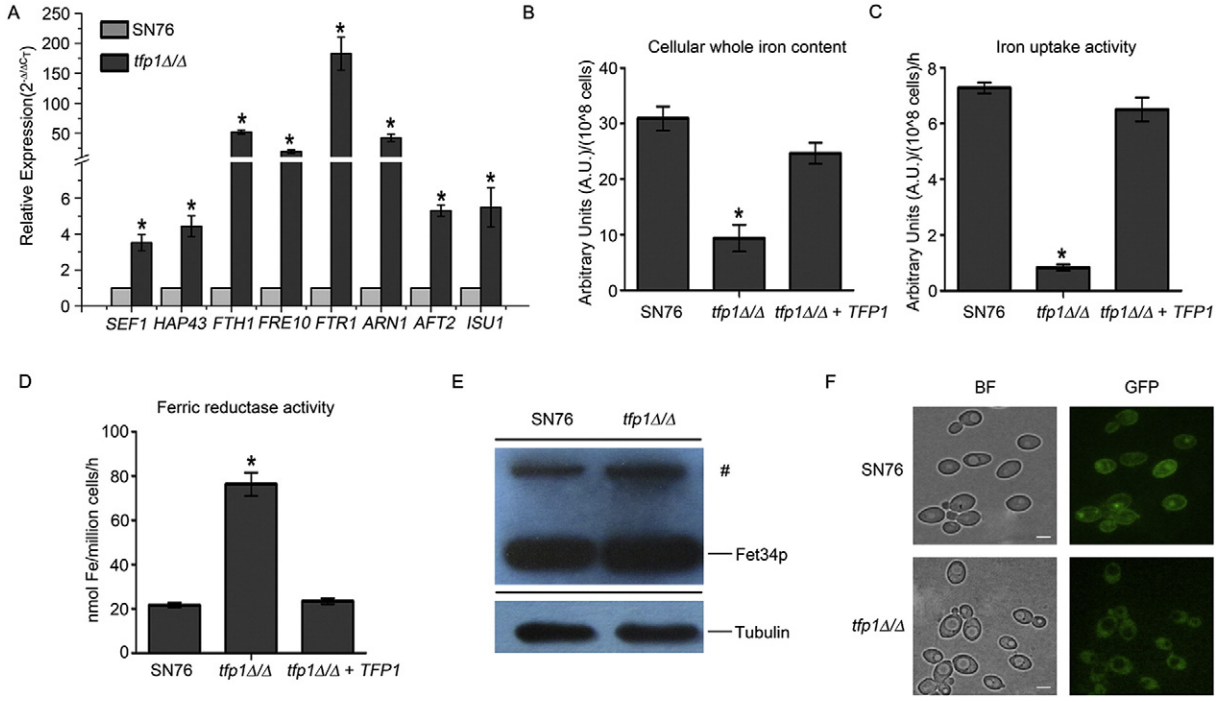


**Fig. 1.** Deletion of *TFP1* generates an iron deprivation signal in *C. albicans*. (A) qRT-PCR analysis of the relative expression levels of iron-related genes that were normalized to the expression of *ACT1* in both strains. (B–D) Cellular whole iron content, iron uptake capacity and ferric reductase activity were measured in the three strains. Data were shown as means ± SD. (E–F) Protein expression and localization of Fet34p were analyzed in SN76 and the *tfp1*Δ/Δ mutant. # indicates a putative Fet-HA N-linked glycosylated product. Bar, 5 μm. (G) The total copper levels were measured by ICP-MS. (H) The growth of three strains was observed on low copper and high copper. (I) Relative mRNA levels of the copper-related genes were analyzed. (J) The total iron content in the *tfp1*Δ/Δ mutant was observed after copper addition. (K) PPD oxidase activity was measured in the *tfp1*Δ/Δ mutant after the addition of copper. (L) Addition of copper could rescue the growth defect of *tfp1*Δ/Δ mutant on iron-limited medium. *, Significant difference ($P < 0.05$) between the *tfp1*Δ/Δ mutant and control strains.

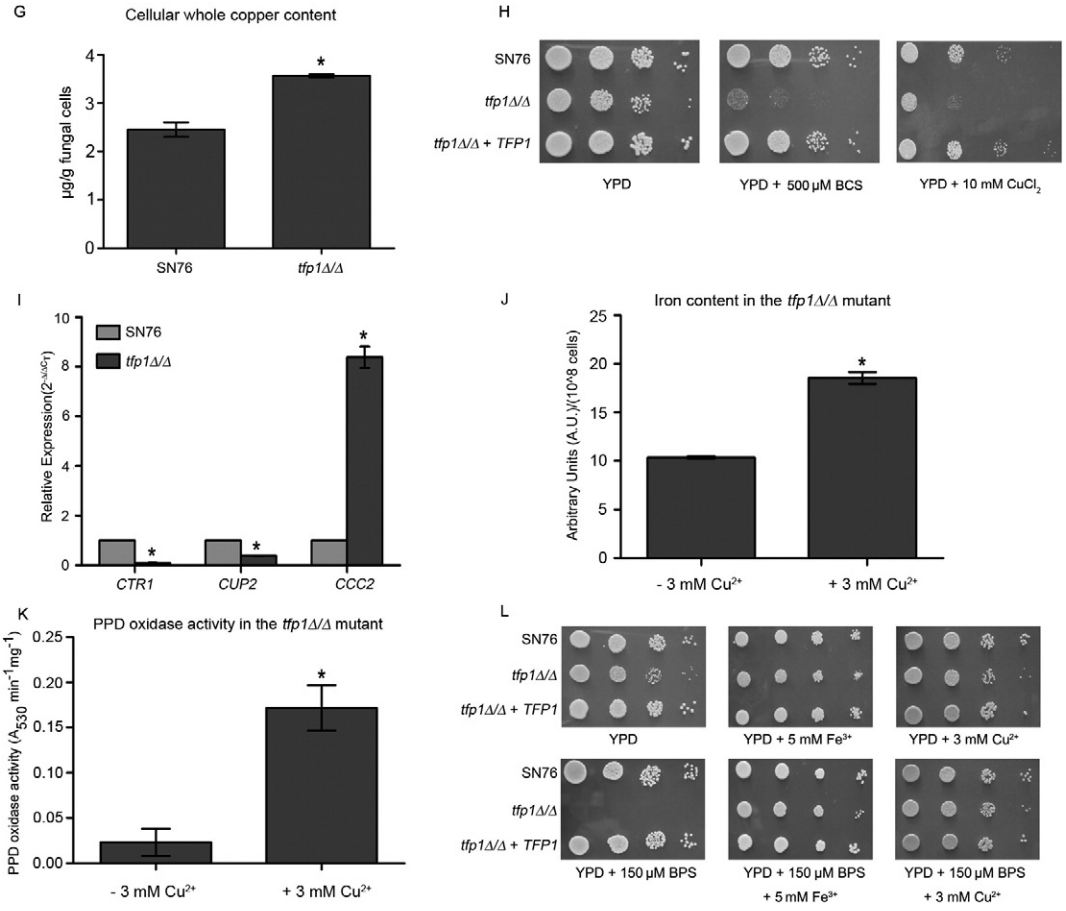


**Fig. 1** (*continued*).

affects copper homeostasis. What's more, the changed expression levels of copper-related genes, such as *CTR1* (copper transporter), *CUP2* (putative copper-binding transcription factor), and *CCC2* (copper-transporting P-type ATPase of Golgi), also reflected the alteration of copper homeostasis in the *tfp1*Δ/Δ mutant (Fig. 1I). Interestingly, though deletion of *TFP1* led to an increase in copper homeostasis, copper supplementation could significantly elevate the iron content (Fig. 1J) and oxidation activity of PPD, an organic substrate used as an oxidase indicator (Fig. 1K), in the *tfp1*Δ/Δ mutant. And spot assay showed that the growth defect of the *tfp1*Δ/Δ mutant on low iron medium could be overcome by addition of iron or copper to the medium (Fig. 1L), further confirming that the defective high affinity iron transport system of the *tfp1*Δ/Δ mutant was in association with the blocked incorporation of copper into Fet34p due to disorders in copper homeostasis. In addition, we observed that iron addition also increased intracellular iron levels in the *tfp1*Δ/Δ mutant (Fig. S1), which is similar to the effect of copper addition. Taken together, deletion of *TFP1* affected copper homeostasis that impeded on the delivery of copper to Fet34p, and consequently impacted on the localization of Fet34p and the high-affinity iron uptake system, and eventually reduced iron uptake from the extra-environment.

### 3.2. Iron/copper improves the respiratory growth of the tfp1Δ/Δ mutant

Iron deficiency could compromise the ability of cells to switch from fermentation to respiratory metabolism [38]. To determine whether disruption of *TFP1* affected respiration metabolism, comparative growth analysis was conducted on different nonfermentable carbon sources. We observed that the *tfp1*Δ/Δ mutant grew poorly on these nonfermentable carbon sources, and the growth defect could be rescued to some extent by iron addition (Fig. 2A). To confirm whether the growth defect was due to iron depletion, we measured total iron levels of the strains grown in YPG medium and found that the total iron content was low in the *tfp1*Δ/Δ mutant as expected (Fig. 2B). The above study has demonstrated that iron addition could elevate total iron levels in the *tfp1*Δ/Δ mutant, further confirming that the defective growth was attributed to iron deficiency. It is reported that the key TCA-cycle enzyme aconitase activity is decreased under iron-limited media [21,39]. Our result also showed that the aconitase activity in the *tfp1*Δ/Δ mutant was decreased, approximately 25% of the control strains (Fig. 2C). The above findings have demonstrated that copper addition could also increase the iron content in the *tfp1*Δ/Δ mutant. In addition, copper is an essential cofactor of cytochrome c oxidase, which is the last enzyme in the respiratory electron chain of mitochondria and is controlled by copper homeostasis [40]. Therefore, the respiratory growth defect of the *tfp1*Δ/Δ mutant was presumed to be also rescued by the addition of copper. As anticipated, we observed that copper supplement partly restored the growth of the *tfp1*Δ/Δ mutant on nonfermentable carbon sources (Fig. 2D). To sum up, more iron or copper was required for respiratory growth of the *tfp1*Δ/Δ mutant.

### 3.3. Tfp1 contributes to the maintenance of cytosolic calcium levels

In *S. cerevisiae*, V-ATPase is important for maintenance of cytosolic calcium homeostasis [41]. Tfp1, as a putative subunit of the vacuolar proton pump, was also related to calcium homeostasis in *C. albicans* [7]. To further investigate the potential mechanism that Tfp1 was involved in calcium homeostasis, the cytosolic calcium levels were

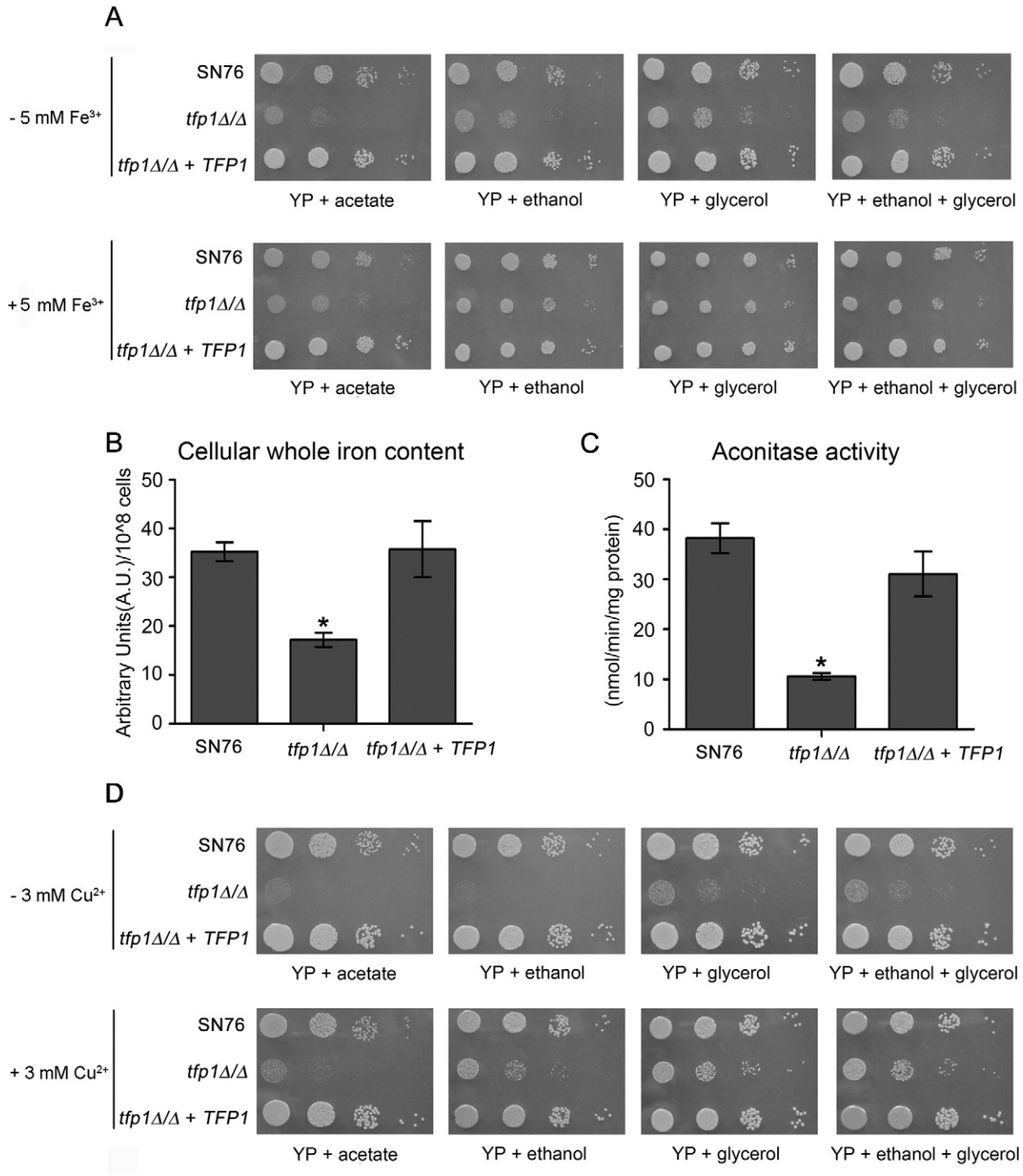


**Fig. 2.** Iron/copper improves respiratory growth of the *tfp1*Δ/Δ mutant. (A) The growth of wild-type strain SN76, *tfp1*Δ/Δ mutant and complemented strain was observed on nonfermentable carbon sources (with or without addition of iron). (B) The total iron levels were measured in the three strains grown in YPG medium. (C) Aconitase activity was analyzed in the three strains grown in YPG medium. * indicates significance at $P < 0.05$. (D) The growth defect of *tfp1*Δ/Δ mutant could be rescued partly by copper addition.

measured upon deletion of *TFP1*. The results showed that cytosolic calcium levels were significantly increased in the *tfp1*Δ/Δ mutant both in normal (YPD) and low calcium (YPD supplemented with 3 mM EGTA) medium (Fig. 3A). Moreover, the addition of EGTA, a calcium chelator, remarkably increased cytosolic calcium levels in the *tfp1*Δ/Δ mutant. In addition, EGTA concentration-kill analyses showed that the inhibitory effect of EGTA was gradually enhanced with its concentration increasing, and 2 mM EGTA was enough to significantly inhibit the growth of the *tfp1*Δ/Δ mutant (Fig. 3B). To elucidate the mechanism, we examined the expression levels of calcium transporter genes by qRT-PCR analysis. The real-time analysis exhibited that the expression levels of plasma membrane calcium channel *CCH1* and *MID1*, the vacuolar membrane calcium pump *PMC1* and the vacuolar membrane calcium channel *YVC1* were up-regulated (Fig. 3C). In addition, attention should be paid to that the expression levels of *VCX1* were not affected, indicating that Tfp1 did not affect Vcx1 at transcriptional level. The up-regulation of *PMC1* and much higher cytosolic calcium levels in the double mutant *tfp1*Δ/Δ*pmc1*Δ/Δ (Fig. 3D) indicated that the deletion of *TFP1* triggered compensatory activation of Pmc1, just like in *S. cerevisiae* V-ATPase mutants [41]. However, the whole calcium levels

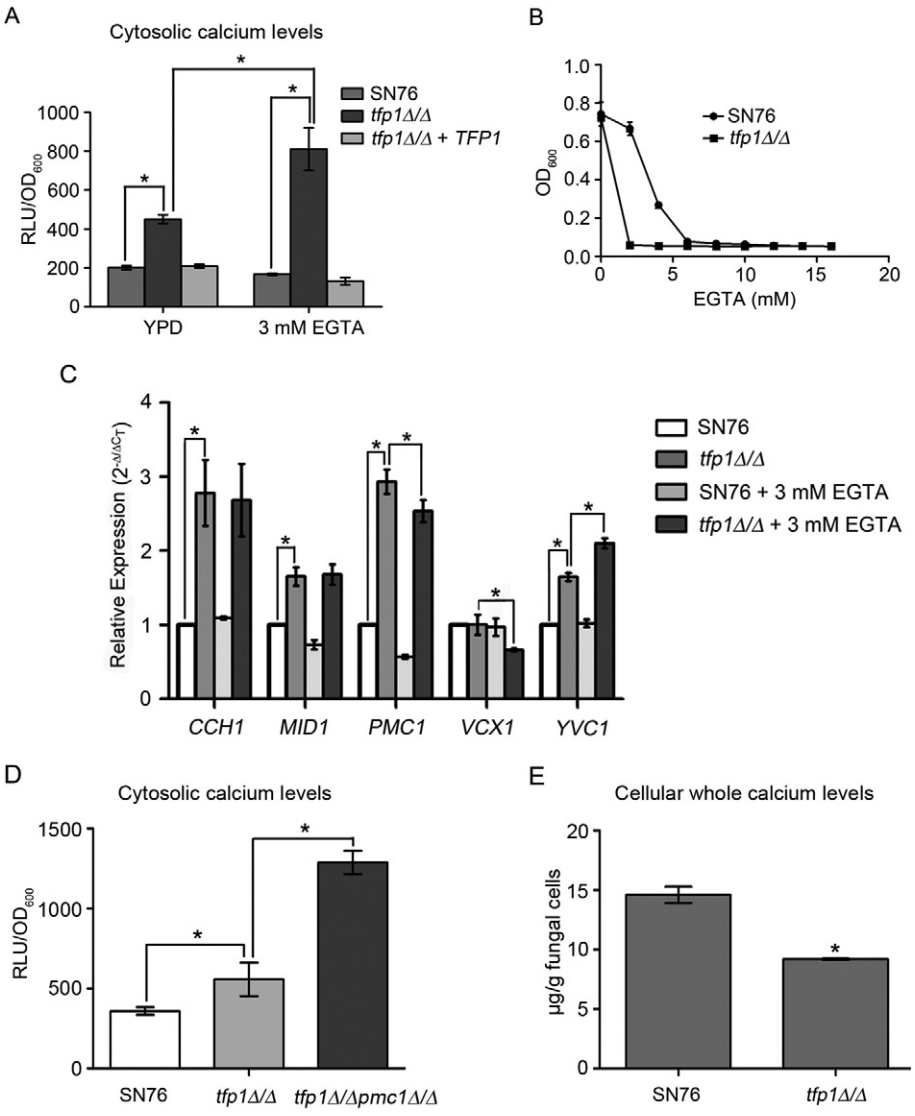


**Fig. 3.** Tfp1 contributes to the maintenance of cytosolic calcium levels. (A) Cytosolic calcium levels were observed in the three strains grown in normal (YPD) and low (YPD supplemented with 3 mM EGTA) calcium medium. (B) EGTA concentration-kill curve was determined in SN76 and the *tfp1*Δ/Δ mutant. (C) The expression levels of calcium transport-related genes were measured as the ratio relative to the nuclear target *ACT1* gene in both strains. (D) Cytosolic calcium levels were measured in SN76, *tfp1*Δ/Δ and *tfp1*Δ/Δ*pmc1*Δ/Δ mutants. (E) The cellular whole calcium levels were determined by ICP-MS analysis. * indicates significance at $P < 0.05$.

in the *tfp1*Δ/Δ mutant were reduced (Fig. 3E), suggesting that the elevated cytosolic calcium levels mainly result from the release of internal stores. When EGTA was added to YPD medium and chelated the extra-environment calcium ion, the expression levels of *PMC1* and *VCX1* in the *tfp1*Δ/Δ mutant were reduced, and the expression levels of *YVC1* were increased compared with YPD medium, suggesting that EGTA addition further induced calcium release from intracellular stores, and caused much higher cytosolic calcium levels and growth toxicity in the *tfp1*Δ/Δ mutant.

### 3.4. Cytosolic calcium status is related to Vcx1 activity

In *S. cerevisiae*, loss of Vcx1 activity results in elevated cytosolic calcium levels in V-ATPase deficient cells [41]. In our study, the *tfp1*Δ/Δ mutant also exhibited high levels of cytosolic calcium. To clarify whether the activity of calcium transporter Vcx1 was affected by Tfp1 in *C. albicans*, the homozygous *vcx1*Δ/Δ was constructed. Our results showed that the cytosolic calcium response of the *vcx1*Δ/Δ mutant to an alkaline stimulus was similar to that of the *tfp1*Δ/Δ mutant (Fig. 4B, C). Both strains exhibited a slow incomplete removal of the elevated cytosolic calcium within 300 s, which was significantly different from the wild-type strain. The wild-type strain displayed a very fast removal of the peak calcium and restored to the normal calcium level within 200 s (Fig. 4A). Therefore, we speculated that loss of Tfp1 might affect cytosolic calcium fluctuation through regulating Vcx1p activity. In order to further confirm the hypothesis, *VCX1* was overexpressed in the wild-type and *tfp1*Δ/Δ strains. As expected, the cytosolic calcium levels in the *tfp1*Δ/Δ mutant with overexpressed *VCX1* reached the same extent as the wild-type strain (Fig. 4D). Taken together, we could conclude that disruption of *TFP1* affected the activity of Vcx1.

### 3.5. The *tfp1*Δ/Δ mutant is sensitive to azole drugs

Previous study reveals that the dysregulation of cellular ion homeostasis is closely associated with fluconazole sensitivity [42]. Moreover, the mutants defective in V-ATPase activity exhibit increased sensitivity to azoles antifungal agents in *Schizosaccharomyces pombe* [43]. The above findings have shown that the putative *C. albicans* V-ATPase subunit Tfp1 was also essential for the maintenance of cellular iron/copper/calcium homeostasis. Therefore, it is of interest to investigate

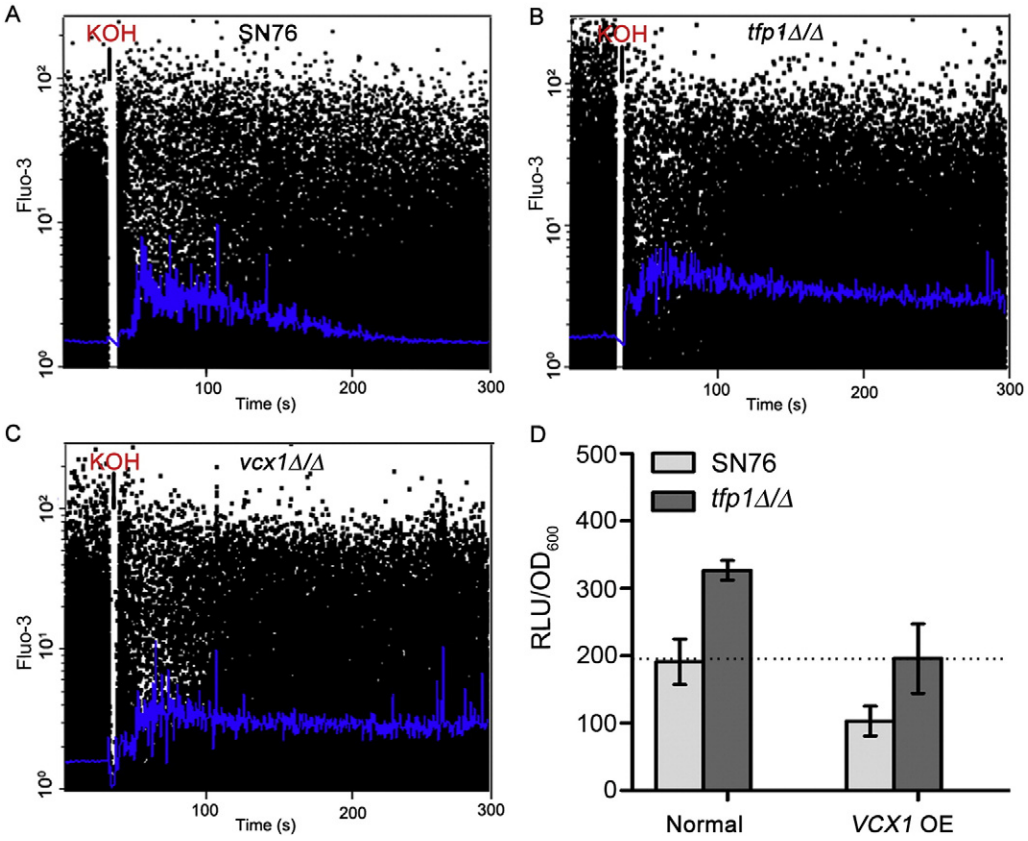


**Fig. 4.** Elevation in cytosolic calcium levels is related to loss of Vcx1 activity. (A–C) The kinetics of cytosolic calcium response to an alkaline stimulus was measured in wild-type strain SN76 (A), the *tfp1*Δ/Δ mutant (B), the *vcx1*Δ/Δ mutant (C). (D) Cytosolic calcium levels were determined in the wild-type strain SN76 and the *tfp1*Δ/Δ mutant with or without overexpression of *VCX1*.

the correlation between Tfp1 and azole antifungal susceptibility. The fluconazole sensitivity of *tfp1*Δ/Δ cells was validated by two different assays. The spot analysis showed that the *tfp1*Δ/Δ mutant was sensitive to fluconazole and terbinafine (Fig. 5A), which function by targeting the enzymes of ergosterol biosynthesis pathway. In addition, the fluconazole sensitivity of the *tfp1*Δ/Δ cells was further characterized by concentration-kill analyses (Fig. 5B). With the concentrations of fluconazole increasing, the growth ability of the three strains was gradually decreased, and the *tfp1*Δ/Δ mutant was significantly attenuated for growth. To investigate the molecular mechanism of fluconazole sensitivity in the *tfp1*Δ/Δ mutant, three factors might be involved.

The primary targets of fluconazole and terbinafine are enzymes of ergosterol biosynthetic pathway, Erg11 and Erg3, respectively [39]. Overexpression or point mutation of *ERG11* confers fluconazole resistance [41,42]. Defective sterol C5, 6 desaturase encoded by *ERG3* has been also considered to be one of the azole resistance mechanisms in *C. albicans* [44]. Ergosterol biosynthesis genes *ERG1*, *ERG3*, and *ERG11* are the most significant genes involved in the resistance to azoles. Therefore, we measured *ERG1*, *ERG3* and *ERG11* mRNA abundance by qRT-PCR. Gene expression data analysis indicated that deletion of *TFP1* caused down-regulation of *ERG1* and *ERG11*, and up-regulation of *ERG3* (Fig. 5C), suggesting that the fluconazole sensitivity of the *tfp1*Δ/Δ mutant was closely related to ergosterol synthesis. In addition, ergosterol is required for cell membrane integrity [45]. The result was also further confirmed by the spot assay that the *tfp1*Δ/Δ mutant was sensitive to membrane-targeting antimicrobial agent SDS (Fig. 5D).

Besides, another significant mechanism of azole sensitivity is a decreased activity of membrane-proteins that efflux the drugs [46]. There are two main classes of efflux proteins in *C. albicans*, the ATP-binding cassette (ABC) pumps and the major facilitator superfamily (MFS) transporters [47]. Clinically relevant azole sensitivity is most often associated with decreased expression of mRNAs for the ABC genes *CaCDR1* and *CaCDR2* [48]. To study the effect of *TFP1* disruption on drug efflux pump activity, we measured the expression of *CDR1* and *MDR1*. The result showed that the expression of *CDR1* was down-regulated compared with the wild-type strain (Fig. 5E). On the contrary, transcript levels of *MDR1* were significantly higher in the *tfp1*Δ/Δ mutant (Fig. 5E), which was in line with the previous report wherein up-regulation of *MDR1* in a petite mutant strain of *C. albicans* was documented [49]. To study the efflux activity of *CDR1* pumps, the ability to efflux rhodamine 6G (R6G), a substrate of *CDR1* pumps, was analyzed in the *tfp1*Δ/Δ mutant [50]. Without glucose addition, no R6G efflux was observed in both strains. Upon the addition of glucose, an increase in Abs (527 nm) value was observed from 0.04 to 0.19 in 10 min in the wild type strain. In contrast, the *tfp1*Δ/Δ mutant exhibited an increase from 0.04 to 0.13 in 10 min, indicating that the mutant had a partial deficiency in R6G efflux, probably due to the reduced activity of *CDR1* pumps.

In addition to the association of fluconazole sensitivity with the ergosterol biosynthesis and drug efflux capacity, dysregulation of ion homeostasis caused by fluconazole might be another reason [42,51]. Previous study has indicated that V-ATPase is the dominant proton pump at endomembrane and plays an important role for the regulation of ion homeostasis [52]. Therefore, we anticipated that the fluconazole sensitivity might be associated with imbalance in ion homeostasis in the *tfp1*Δ/Δ mutant. To confirm the hypothesis, we measured the expression changes of iron and calcium-related genes in response to fluconazole. The expression levels of *CFL1*, *FRE10*, *FTR1*, *VCX1* and *PMR1* were up-regulated in the wild type strain when treated with fluconazole, but could not respond to the same extent when *TFP1* was disrupted (Fig. 6). In addition, the expression change of *RTA2* was significantly low

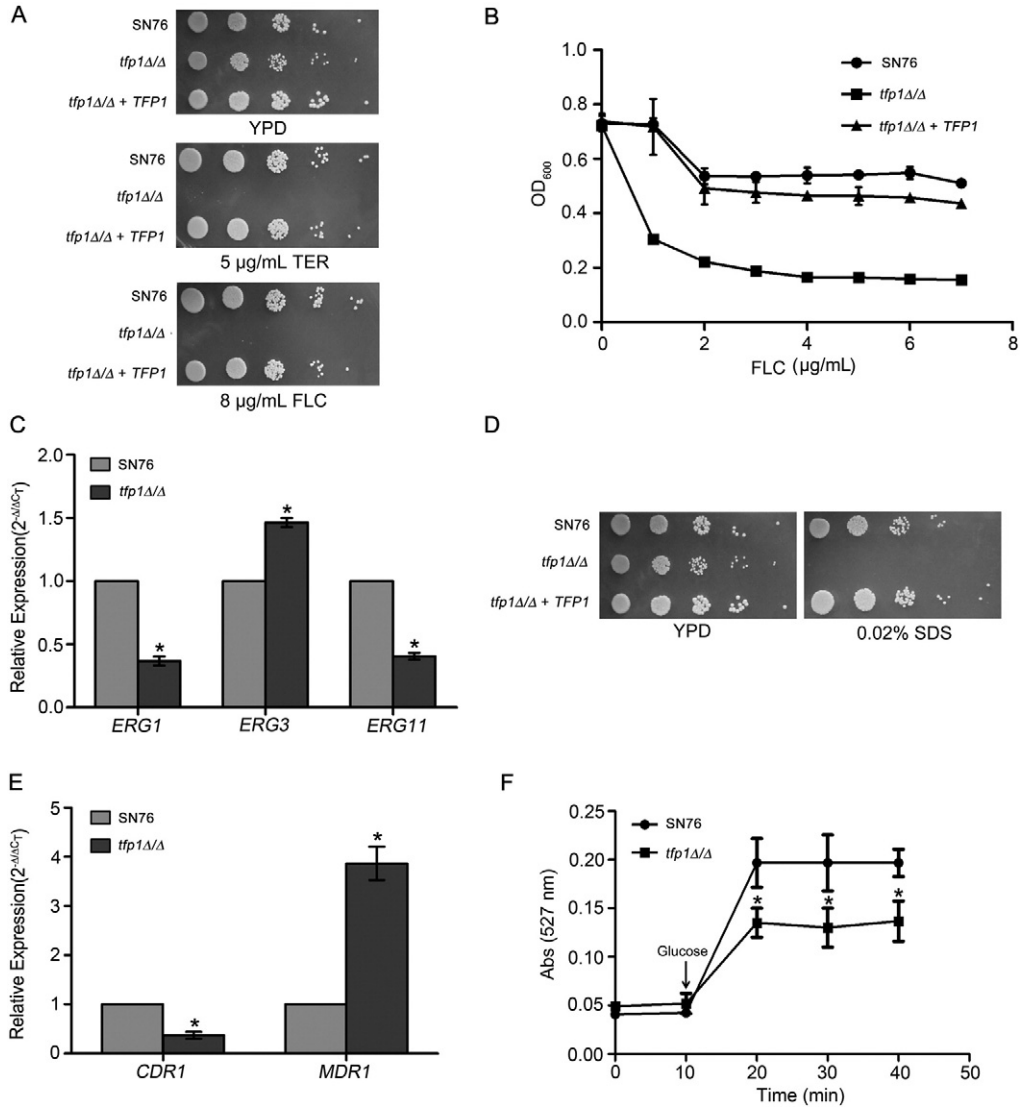


**Fig. 5.** The *tfp1*Δ/Δ mutant was sensitive to fluconazole. (A) The three strains were spotted onto YPD plates supplemented with fluconazole (FLC) or terbinafine (TER) at the indicated concentrations. Cells were photographed after two days of incubation at 30 °C. (B) Fluconazole concentration-kill curve was measured in SN76, the *tfp1*Δ/Δ mutant and the complemented strain. (C) The expression levels of ergosterol biosynthesis genes (*ERG1*, *ERG3* and *ERG11*) were determined by qRT-PCR analysis. (D) Growth phenotype of the *tfp1*Δ/Δ mutant was observed under membrane-targeting agent SDS. (E) Relative levels of *CDR1* and *MDR1* were analyzed in the *tfp1*Δ/Δ mutant compared to the wild-type strain. (F) Efflux of fluorescent R6G, a substrate of *CDR1* pumps, was measured in the wild-type and *tfp1*Δ/Δ strains.

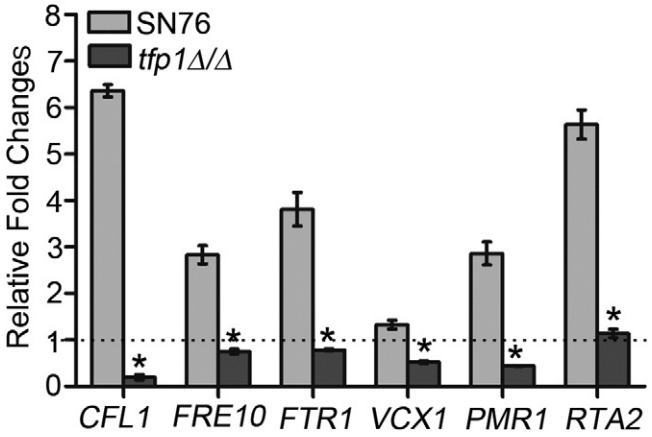


**Fig. 6.** Relative fold changes of iron and calcium transport genes were determined in response to fluconazole treatment in both strains.

in the *tfp1*Δ/Δ mutant compared with the wild-type strain in response to fluconazole. The disruption of *RTA2* could block the emergence of calcium-mediated tolerance to fluconazole by aggravating its impairment to the plasma membrane of *C. albicans* [53]. Taken together, these data suggested that the enhanced sensitivity of the *tfp1*Δ/Δ mutant to fluconazole may be due to dysregulation of iron and calcium homeostasis, in addition to the reduced ergosterol content and *CDR1* efflux pump activity.

### 3.6. The *tfp1*Δ/Δ mutant impairs in the utilization of GlcNAc

In *S. coelicolor*, GlcNAc utilization regulator, DasR, could transcriptionally repress the iron utilization repressor dmdR1 to control siderophore production, providing a link between nutrient and metal ion [54]. To further explore the potential role of *TFP1* in *C. albicans*, we tested the growth of *C. albicans* strains on different carbon source plates. The result showed that there were no significant differences in carbon metabolism between the wild-type and *tfp1*Δ/Δ mutant strains except for GlcNAc (Fig. 7A). Therefore, we anticipated that the growth defect

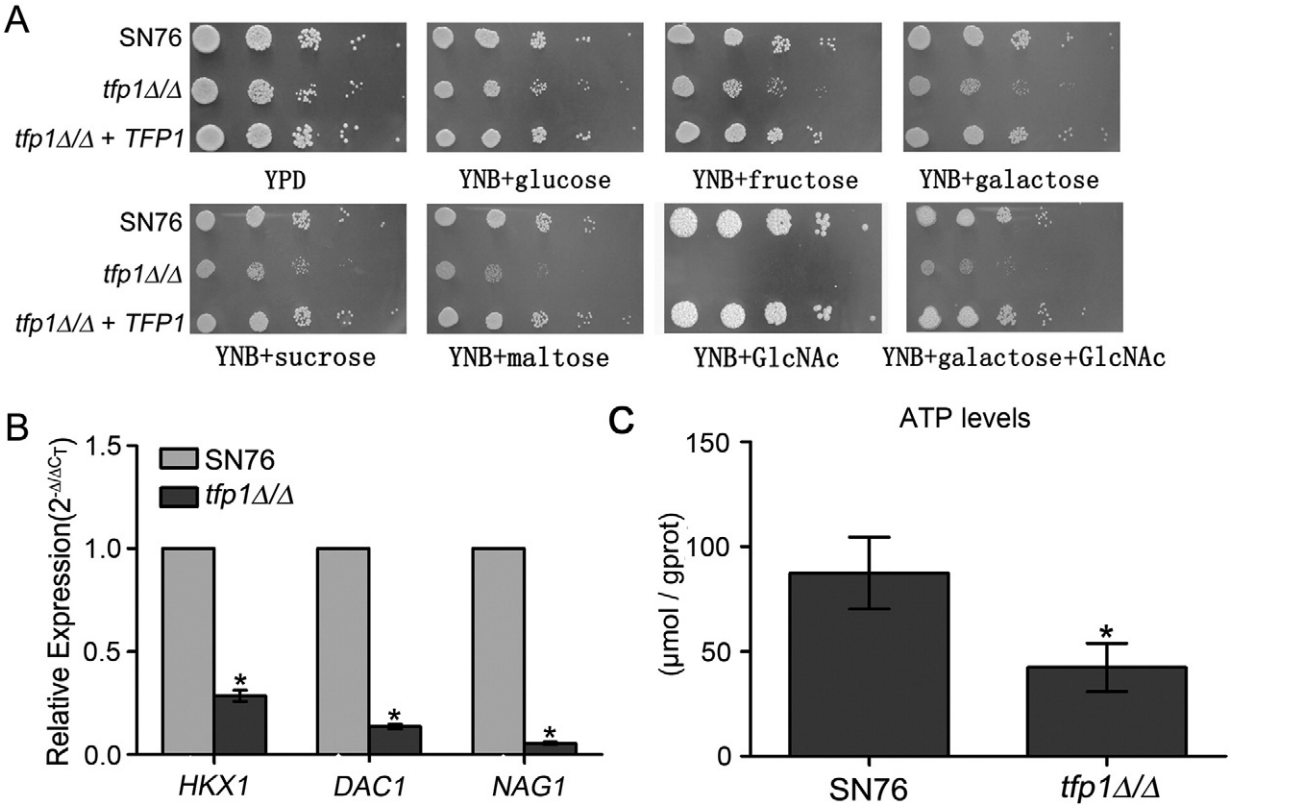


**Fig. 7.** The *tfp1*Δ/Δ mutant was unable to utilize GlcNAc as sole carbon source. (A) Growth of the three strains was observed on different carbon sources. (B) Relative expression levels of GlcNAc catabolic genes were analyzed by qRT-PCR. (C) Cellular ATP levels were measured in both strains after treatment by GlcNAc for 6 h. *, Significant difference ($P < 0.05$) between the *tfp1*Δ/Δ mutant and wild-type strain SN76.

of the *tfp1*Δ/Δ mutant on GlcNAc might be associated with iron uptake. To verify the assumption, we observed the growth of the *tfp1*Δ/Δ mutant on GlcNAc plate supplemented with iron, the result showed that the growth defect of the *tfp1*Δ/Δ mutant was not rescued by iron addition (data not shown). Hence, reasons for this phenotype may be explained from three other aspects. First, the *tfp1*Δ/Δ mutant might be unable to take up GlcNAc; second, GlcNAc or its derivatives may be toxic to the *tfp1*Δ/Δ mutant; third, GlcNAc could not be catabolized by the *tfp1*Δ/Δ mutant. To validate these hypotheses, we observed the localization of GlcNAc specific transporter Ngt1. The images unveiled that Ngt1 was normally localized on the plasma membrane in the *tfp1* Δ/Δ mutant, and the overexpression of *NGT1* failed to rescue the growth defect (data not shown), revealing that deletion of *TFP1* did not affect GlcNAc transporter, Ngt1. To demonstrate the second aspect, we observed the growth of *tfp1*Δ/Δ mutant on galactose plus GlcNAc. The result showed that the *tfp1*Δ/Δ mutant can survive on the plate, suggesting that GlcNAc or its derivative was not toxic. To confirm the third speculation, we measured the expression levels of the enzymes of GlcNAc catabolic pathway by qRT-PCR. The result showed that the expression levels of three main enzymes, including *HKX1*, *DAC1* and *NAG1*, were all down-regulated compared with the wild-type strain (Fig. 7B). Further study found that the ATP levels were significantly decreased in the *tfp1*Δ/Δ mutant after treatment by GlcNAc for 6 h (Fig. 7C). Therefore, ATP depletion due to the decreased ability to catabolize GlcNAc might be responsible for growth defect of the *tfp1*Δ/Δ mutant on GlcNAc agar plate.

## 4. Discussion

As an important proton pump, V-ATPase plays essential roles in many cellular processes, including both vacuolar acidification related functions (canonical roles) and other roles that are not readily attributable to its proton-motive activity (non-canonical roles) [55,56]. The canonical functions, such as endocytic traffic, protein processing and degradation and so on, are well documented. However, the non-canonical roles, including membrane fusion, scaffold for protein–protein interactions and so on, are still poorly understood, which need further investigation. Therefore, the effects of loss of V-ATPase were far-reaching and may be involved in a complex network. In this study, we investigated the functions of a putative V-ATPase subunit Tfp1 in cellular ion homeostasis, fluconazole resistance and GlcNAc utilization, which provides new insights into the functional roles of V-ATPase.

### 4.1. Tfp1 is required for ion homeostasis

It is known that V-ATPase plays an important role in the control of pH and ionic homeostasis in eukaryotes [57]. In *Histoplasma capsulatum*, the V-ATPase mutants do not grow on iron-limited medium [58]. Previous studies concluded that several kinds of mutants of *S. cerevisiae* were unable to grow on iron-restricted medium, including mutants that are defective in the structural components of the high affinity iron uptake system [21], the assembly of the transport system [59], or vacuolar trafficking or acidification [10,60]. In *S. cerevisiae*, the *vma2*Δ mutant generates an iron deprivation signal that is alleviated by induction of *TAS2* [11]. In our study, we found that deletion of *TFP1* resulted in the inability to grow on low iron medium, and generated an iron starvation signal with reduced iron levels and iron uptake capacity. Further study demonstrated that the decreased iron uptake might be attributed to mislocalization of multicopper oxidase Fet34p, which was associated with disorders in copper homeostasis. In the mutants of *S. cerevisiae* that exhibit a low iron growth defect, its apoFet3 could be transported to the cell surface but has no enzyme activity [10,60]. However, it is

equally true that defective multicopper oxidase compromised the ability of strains to grow on iron-limited medium in both *S. cerevisiae* and *C. albicans* mutants [35,60]. Previous study demonstrates that activation of multicopper oxidase requires copper loading [60], which requires normal copper homeostasis and acidification of post-Golgi vesicular compartments [10]. In our study, we found that deletion of *TFP1* caused disorders in copper homeostasis. However, copper addition could elevate multicopper oxidase activity and iron levels in the *tfp1*Δ/Δ mutant, as well as overcome the growth defect on low iron. Hence, iron uptake was closely associated with copper homeostasis in the *tfp1*Δ/Δ mutant. It is reported that the pH gradient across the vacuolar membrane plays a critical role in maintaining optimal copper homeostasis [61], and the delivery of copper to multicopper oxidase requires acidification of post-Golgi vesicular compartments, which is dependent on the vacuolar $H^+$-ATPase [10]. Therefore, loss of V-ATPase activity might cause both disorders in copper homeostasis and compromised copper delivery, as well as reduced acidification of post-Golgi vesicular compartments, and finally affects functions of Fet34p and high-affinity iron uptake.

The TCA cycle and electron transport chain should be negatively affected by iron depletion because these processes depend on specific iron-containing enzymes [21]. In *C. neoformans cfo1* mutant, iron depletion compromises the growth and aconitase activity on nonfermentable carbon sources that were in line with our study [21]. In our study, the growth defect of *tfp1*Δ/Δ cells was partly rescued by iron addition, suggesting that the growth defect was related to iron availability. In addition, copper addition could also restore the growth of the *tfp1*Δ/Δ mutant to some extent, which was likely due to elevated iron content or cytochrome c oxidase. However, the *cls*Δ mutants of *S. cerevisiae* that are unable to grow on nonfermentable carbon sources have normal rates of respiration and normal levels of several respiratory chain enzymes in isolated mitochondria [62], which was not in agreement with our results. In our study, the cellular iron levels were reduced in the *tfp1*Δ/Δ mutant, which may explain the compromised aconitase activity. Since the iron levels in the *cls*Δ and *vma2*Δ mutants of *S. cerevisiae* are either not measured or not altered.

In addition to iron and copper homeostasis, disruption of *TFP1* also led to a disturbance of calcium homeostasis manifested by decreased total calcium content and elevated cytosolic calcium levels, growth inhibition by EGTA addition, and sensitivity to high calcium concentrations [7]. Further study found that disruption of *TFP1* affected calcium-related transporters expression and/or activity. First, the *tfp1*Δ/Δ mutant exhibited reduced total calcium levels, suggesting that the function of the high-affinity calcium uptake system was affected. And the elevated cytosolic calcium concentration in the *tfp1*Δ/Δ mutant was due to calcium release from internal stores. Second, *TFP1* disruption up-regulated *PMC1*, suggesting that loss of V-ATPase caused compensatory up-regulation of *PMC1* that was consistent with previous report [41]. This conclusion was further confirmed by the significantly elevated cytosolic calcium levels in the double mutant *tfp1*Δ/Δ *pmc1*Δ/Δ. Third, the expression levels of *VCX1* were not affected upon deletion of *TFP1,* indicating that *VCX1* was not mediated by Tfp1 at transcriptional level. EGTA addition further increased cytosolic calcium levels in the *tfp1*Δ/Δ mutant, which was related to down-regulation of *PMC1* and *VCX1* and up-regulation of *YVC1* in low calcium medium compared with in normal calcium medium. In *S. cerevisiae*, the elevated cytosolic calcium levels reported to V-ATPase mutants have been attributed to loss of Vcx1 activity [41]. In our study, kinetics of cytosolic calcium response to an alkaline stimulus exhibited that the response of *vcx1*Δ/Δ mutant was similar to that of *tfp1*Δ/Δ mutant. Moreover, overexpression of *VCX1* in the *tfp1* Δ/Δ mutant decreased cytosolic calcium to wild-type levels. These results indicate that calcium status in the *tfp1*Δ/Δ mutant was closely related to Vcx1 activity. However, the *vcx1*Δ/Δ mutant did not show calcium sensitivity and significantly elevated cytosolic calcium (data not shown), indicating that there are additional complexities in the role of Tfp1 in calcium homeostasis maintenance.

In addition, the inhibitor of vacuolar acidification, chloroquine, also led to decreased total iron content (Fig. S2A) and elevated cytosolic calcium levels (Fig. S2B) in the wild-type strain, indicating that the disorders in ion homeostasis may be associated with defective vacuolar acidification.

### 4.2. Deletion of TFP1 leads to sensitivity to fluconazole

Fluconazole is one of the most commonly prescribed antifungal drugs for the treatment of fungal infections, which targets the biosynthesis of ergosterol that is the main sterol of fungal membranes [63]. In our study, the *tfp1*Δ/Δ mutant exhibited hypersensitivity to fluconazole and terbinafine, and expression changes of three key enzymes in ergosterol synthesis pathway, including Erg1, Erg3 and Erg11. *ERG1* and *ERG11* were down-regulated and *ERG3* was up-regulated. There are reports that iron deprivation results in up-regulations of *ERG3* and down-regulation of *ERG11,* finally leads to lowering of ergosterol content [24,64]. Therefore, the reduced iron levels in the *tfp1*Δ/Δ mutant may contribute to the expression alteration of these genes, and further led to fluconazole sensitivity. In addition, a recent study has identified V-ATPase as a major downstream target of widely used azole drug, and demonstrates that the antifungal activity of azole affects V-ATPase function through impeding on ergosterol biosynthesis [6]. Vice versa, our study indicates that V-ATPase function is required for ergosterol biosynthesis and tolerance of azole, suggesting that V-ATPase and antifungal activity of azole have an influence on each other.

Overexpression of drug efflux pump is another well-known mechanism for the development of fluconazole resistance in *C. albicans* [65]. Our results showed that deletion of *TFP1* led to up-regulation of *MDR1* and down-regulation of *CDR1*. The R6G efflux test unveiled reduced efflux activity of *CDR1* pumps in the *tfp1*Δ/Δ mutant. Therefore, the sensitivity of the *tfp1*Δ/Δ mutant to fluconazole may be also associated with the decreased *CDR1* pump efflux activity. Some mutants that affect the high affinity iron uptake show an increased sensitivity to fluconazole independent of efflux pump proteins, Cdr1 and Cdr2 [24], which is inconsistent with our results. It might be due to that loss of *TFP1* affects more cellular processes other than iron homeostasis. In mammalian cells, iron depletion leads to the activation of *MDR1* mediated by hypoxia inducible factor-1 (*HIF-1*) [66,67]. Therefore, the up-regulation of *MDR1* may be attributed to low iron levels in the *tfp1*Δ/Δ mutant. In brief, the reduced *CDR1* efflux capacity is another underlying mechanism by which disruption of *TFP1* causes fluconazole susceptibility.

The effect of fluconazole plus cationic drug treatment was enhanced by the malfunction of alkali-metal-cation transporters that contribute to the regulation of membrane potential and cation homeostasis [68]. Vasicek et al. observed that an *upc2*Δ/Δ mutant, defective in regulating the expression of genes involved in ergosterol biosynthesis, exhibited enhanced susceptibility to fluconazole [42]. Furthermore, mRNA analysis unveils that fluconazole exposure results in down-regulation of high-affinity iron uptake genes upon deletion of *UPC2*. In addition, mutants defective in high affinity iron uptake also displayed enhanced susceptibility to fluconazole [21,24]. In *S. cerevisiae* and *C. albicans*, amiodarone sensitivity correlates with cytosolic calcium overload, and low doses of amiodarone and fluconazole are strongly synergistic and exhibit potent fungicidal effects in combination [6,69], which was similar to the elevated cytosolic levels in the *tfp1*Δ/Δ mutant. In the present study, we found that when *TFP1* is intact, fluconazole exposure results in up-regulation of six genes related to iron and calcium uptake or homeostasis (*CFL1*, *FRE10*, *FTR1*, *VCX1* and *PMR1*). When *TFP1* is disrupted, fluconazole exposure results in down-regulation of these genes, suggesting that *TFP1* might be required for these processes. Therefore, we speculated that fluconazole sensitivity of the *tfp1*Δ/Δ mutant may be associated with the dysregulation of iron and calcium homeostasis. Besides, the relative fold change of *RTA2* was low in the *tfp1*Δ/Δ mutant in response to fluconazole, which was associated with azole resistance

in *C. albicans* [51]. Herein, the expression changes of all above genes were in association in azole sensitivity.

Taken together, reduced ergosterol biosynthesis and *CDR1* efflux pump activity, and dysregulation of iron and calcium homeostasis together contribute to fluconazole sensitivity of the *tfp1*Δ/Δ mutant.

### 4.3. Disruption of TFP1 leads to the inability to utilize GlcNAc

In *C. albicans*, there are at least two ways to acquire iron. One is directly through high affinity iron uptake system, and another is through siderophore [70]. In *S. coelicolor*, GlcNAc could inhibit siderophore production [52], indicating that there is a relationship between nutrient and iron. Our study for the first time reported that the putative V-ATPase mutant, the *tfp1*Δ/Δ mutant, was unable to make use of GlcNAc. Further investigation unveiled that it was due to decreased catabolic ability of the *tfp1*Δ/Δ mutant to GlcNAc rather than iron limitation. In addition, we found that the ATP levels were decreased in the *tfp1*Δ/Δ mutant after treatment by GlcNAc for 6 h, further demonstrating that the defective growth of the *tfp1*Δ/Δ mutant on GlcNAc plates was due to depletion of ATP. However, transcription factors involved in controlling GlcNAc catabolic genes are still unclear in *C. albicans*. Thereby, the underlying mechanism by which V-ATPase affected the GlcNAc catabolic enzymes remains to be further investigated.

In consideration of the pleiotropic effects displayed by cells with defective Tfp1, we proposed a simple mode for the functions of Tfp1 (Fig. 8). Tfp1, as a putative subunit of V-ATPase, is involved in maintenance of several types of ion homeostasis, including copper, iron and calcium. Disorders in ion homeostasis further impede on varieties of other cellular processes, such as respiratory growth, fluconazole resistance, and ergosterol biosynthesis. In addition, we for the first time found that deletion of *TFP1* affects GlcNAc metabolism. While previous study reported that there is a correlation between GlcNAc and metal ion, iron addition could not rescue the growth defect, suggesting that Tfp1 might mediate GlcNAc utilization by non-ionic mechanism. While the functions of Tfp1 in ion homeostasis have been delineated to some extent, the role of Tfp1 in non-ionic homeostasis, such as GlcNAc metabolism, remains further investigated. In all, our results add to the list of proteins that may be used as a target to intervene with V-ATPase functions in *C. albicans*.

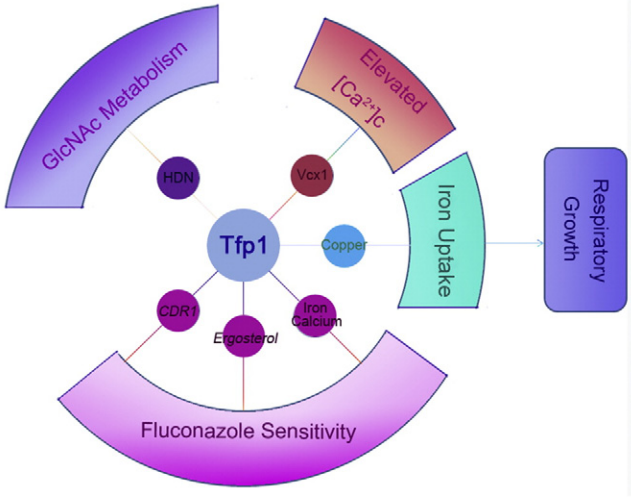


**Fig. 8.** A simple model for the role of Tfp1 in *C. albicans*. Deletion of *TFP1* results in disorders in copper homeostasis, which affects iron uptake. Subsequently, depletion of iron exerts a profound influence on respiratory growth in *C. albicans*. Besides, disruption of *TFP1* leads to elevated cytosolic calcium levels through loss of Vcx1. In addition, the *tfp1*Δ/Δ mutant was hypersensitive to fluconazole through reduced ergosterol biosynthesis and *CDR1* pump activity, and dysregulation of iron and calcium homeostasis. Last but not least, the *tfp1*Δ/Δ mutant was unable to utilize GlcNAc as sole carbon source due to decreased expression levels of *HKX1*, *DAC1*, and *NAG1*. HDN indicates GlcNAc catabolic genes, including *HKX1*, *DAC1*, and *NAG1*.

Supplementary data to this article can be found online at http://dx.doi.org/10.1016/j.bbamcr.2015.08.005.

## Transparency document

The Transparency document associated with this article can be found, in online version.

## Acknowledgments

We are grateful to Dr. Suzanne M. Noble (University of California—San Francisco, USA), Dr. Gerald Fink (Whitehead Institute for Biomedical Research, MIT, USA), Dr. Julia R. Koehler (Boston Children's Hospital, USA) and Dr. P. Brown (University of Aberdeen, UK) for the generous gift of strains and plasmids. This study was supported by the National Natural Science Foundation of China (No. 81471923, No. 81171541 and No. 31400132), the Tianjin Research Program of Application Foundation and Advanced Technology (No. 15JCQNJC09300), the China Postdoctoral Science Foundation (No. 2015T80213) and the Fundamental Research Funds for the Central Universities.

## References

[1] P.M. Kane, The where, when, and how of organelle acidification by the yeast vacuolar $H^+$-ATPase, Microbiol. Mol. Biol. Rev. 70 (2006) 177–191.
[2] S. Breton, D. Brown, New insights into the regulation of V-ATPase-dependent proton secretion, Am. J. Physiol. Renal. 292 (2007) F1–F10.
[3] G.A. Martínez-Muñoz, P. Kane, Vacuolar and plasma membrane proton pumps collaborate to achieve cytosolic pH homeostasis in yeast, J. Biol. Chem. 283 (2008) 20309–20319.
[4] J.M. Pardo, B. Cubero, E.O. Leidi, F.J. Quintero, Alkali cation exchangers: roles in cellular homeostasis and stress tolerance, J. Exp. Bot. 57 (2006) 1181–1199.
[5] Y.Q. Zhang, R. Rao, The V-ATPase as a target for antifungal drugs, Curr. Protein Pept. Sci. 13 (2012) 134–140.
[6] Y.Q. Zhang, R. Rao, Requirement for ergosterol in V-ATPase function underlies antifungal activity of azole drugs, Virulence 1 (2010) 551–554.
[7] C. Jia, Q.L. Yu, N. Xu, B. Zhang, Y.J. Dong, X.H. Ding, Y.L. Chen, B. Zhang, L.J. Xing, M.C. Li, Role of TFP1 in vacuolar acidification, oxidative stress and filamentous development in *Candida albicans*, Fungal Genet. Biol. 71 (2014) 58–67.
[8] C. Askwith, J. Kaplan, An oxidase–permease-based iron transport system in *Schizosaccharomyces pombe* and its expression in *Saccharomyces cerevisiae*, J. Biol. Chem. 272 (1997) 401–405.
[9] A. Singh, S. Severance, N. Kaur, W. Wiltsie, D.J. Kosman, Assembly, activation, and trafficking of the Fet3p·Ftr1p high affinity iron permease complex in *Saccharomyces cerevisiae*, J. Biol. Chem. 281 (2006) 13355–13364.
[10] S.R. Davis-Kaplan, D.M. Ward, S.L. Shiflett, J. Kaplan, Genome-wide analysis of iron-dependent growth reveals a novel yeast gene required for vacuolar acidification, J. Biol. Chem. 279 (2004) 4322–4329.
[11] H.I. Diab, P.M. Kane, Loss of vacuolar $H^+$-ATPase (V-ATPase) activity in yeast generates an iron deprivation signal that Is moderated by induction of the peroxiredoxin TSA2, J. Biol. Chem. 288 (2013) 11366–11377.
[12] S. Groppi, F. Belotti, R.L. Brandão, E. Martegani, R. Tisi, Glucose-induced calcium influx in budding yeast involves a novel calcium transport system and can activate calcineurin, Cell Calcium 49 (2011) 376–386.
[13] J. Linghuo, A. Joerg, W. Jihong, D. Wei, Y. Xuexue, L. Xichuan, S. Dominique, G. Joachim, The *Candida albicans* plasma membrane protein Rch1p, a member of the vertebrate SLC10 carrier family, is a novel regulator of cytosolic $Ca^{2+}$ homoeostasis, Biochem. J. 444 (2012) 497–502.
[14] Q. Yu, F. Wang, Q. Zhao, J. Chen, B. Zhang, X. Ding, H. Wang, B. Yang, G. Lu, B. Zhang, A novel role of the vacuolar calcium channel Yvc1 in stress response, morphogenesis and pathogenicity of *Candida albicans*, Int. J. Med. Microbiol. 304 (2014) 339–350.
[15] S. Bates, D.M. MacCallum, G. Bertram, C.A. Munro, H.B. Hughes, E.T. Buurman, A.J. Brown, F.C. Odds, N.A. Gow, *Candida albicans* Pmr1p, a secretory pathway P-type $Ca^{2+}/Mn^{2+}$-ATPase, is required for glycosylation and virulence, J. Biol. Chem. 280 (2005) 23408–23415.
[16] A. Miseta, R. Kellermayer, D.P. Aiello, L. Fu, D.M. Bedwell, The vacuolar $Ca^{2+}/H^+$ exchanger Vcx1p/Hum1p tightly controls cytosolic $Ca^{2+}$ levels in *S. cerevisiae*, FEBS Lett. 451 (1999) 132–136.
[17] K.W. Cunningham, G.R. Fink, Calcineurin inhibits VCX1-dependent $H^+/Ca^{2+}$ exchange and induces $Ca^{2+}$ ATPases in *Saccharomyces cerevisiae*, Mol. Cell. Biol. 16 (1996) 2226–2237.
[18] X. Ding, Q. Yu, N. Xu, Y. Wang, X. Cheng, K. Qian, Q. Zhao, B. Zhang, L. Xing, M. Li, Ecm7, a regulator of HACS, functions in calcium homeostasis maintenance, oxidative stress response and hyphal development in *Candida albicans*, Fungal Genet. Biol. 57 (2013) 23–32.

[19] M. Spitzer, E. Griffiths, K.M. Blakely, J. Wildenhain, L. Ejim, L. Rossi, G. De Pascale, J. Curak, E. Brown, M. Tyers, Cross-species discovery of syncretic drug combinations that potentiate the antifungal fluconazole, Mol. Syst. Biol. 7 (2011).

[20] L. Yan, M. Li, Y. Cao, P. Gao, Y. Cao, Y. Wang, Y. Jiang, The alternative oxidase of *Candida albicans* causes reduced fluconazole susceptibility, J. Antimicrob. Chemother. 64 (2009) 764–773.

[21] J. Kim, Y.J. Cho, E. Do, J. Choi, G. Hu, B. Cadieux, J. Chun, Y. Lee, J.W. Kronstad, W.H. Jung, A defect in iron uptake enhances the susceptibility of *Cryptococcus neoformans* to azole antifungal drugs, Fungal Genet. Biol. 49 (2012) 955–966.

[22] R. Kaur, I. Castaño, B.P. Cormack, Functional genomic analysis of fluconazole susceptibility in the pathogenic yeast *Candida glabrata*: roles of calcium signaling and mitochondria, Antimicrob. Agents Chemother. 48 (2004) 1600–1613.

[23] J.B. Konopka, N-acetylglucosamine functions in cell signaling, Scientifica 2012 (2012).

[24] T. Prasad, A. Chandra, C.K. Mukhopadhyay, R. Prasad, Unexpected link between iron and drug resistance of *Candida spp.*: iron depletion enhances membrane fluidity and drug diffusion, leading to drug-susceptible cells, Antimicrob. Agents Chemother. 50 (2006) 3597–3606.

[25] T. Naderer, J. Heng, M.J. McConville, Evidence that intracellular stages of *Leishmania major* utilize amino sugars as a major carbon source, PLoS Pathog. 6 (2010) e1001245.

[26] S.M. Noble, A.D. Johnson, Strains and strategies for large-scale gene deletion studies of the diploid human fungal pathogen *Candida albicans*, Eukaryot. Cell 4 (2005) 298–309.

[27] C.D. Zhang, J.B. Konopka, A photostable green fluorescent protein variant for analysis of protein localization in *Candida albicans*, Eukaryot. Cell 9 (2010) 224–226.

[28] X. Cheng, N. Xu, Q. Yu, X. Ding, K. Qian, Q. Zhao, Y. Wang, B. Zhang, L. Xing, M. Li, Novel insight into the expression and function of the multicopper oxidases in *Candida albicans*, Microbiology 159 (2013) 1044–1055.

[29] P.C. Hsu, C.Y. Yang, C.Y. Lan, *Candida albicans* Hap43 is a repressor induced under low-iron conditions and is essential for iron-responsive transcriptional regulation and virulence, Eukaryot. Cell 10 (2011) 207–225.

[30] N. Xu, K. Qian, Y. Dong, Y. Chen, Q. Yu, B. Zhang, L. Xing, M. Li, Novel role of *Candida albicans* ferric reductase gene CFL1 in iron acquisition, oxidative stress tolerance, morphogenesis and virulence, FEMS Yeast Res. 14 (2014) 1037–1047.

[31] N. Xu, Y. Dong, X. Cheng, Q. Yu, K. Qian, J. Mao, C. Jia, X. Ding, B. Zhang, Y. Chen, Cellular iron homeostasis mediated by the Mrs4–Ccc1–Smf3 pathway is essential for mitochondrial function, morphogenesis and virulence in *Candida albicans*, Biochim. Biophys. Acta, Mol. Cell Res. 1843 (2014) 629–639.

[32] A.J. Pierik, D.J. Netz, R. Lill, Analysis of iron–sulfur protein maturation in eukaryotes, Nat. Protoc. 4 (2009) 753–766.

[33] E. Thomas, E. Roman, S. Claypool, N. Manzoor, J. Pla, S.L. Panwar, Mitochondria influence CDR1 efflux pump activity, Hog1-mediated oxidative stress pathway, iron homeostasis, and ergosterol levels in *Candida albicans*, Antimicrob. Agents Chemother. 57 (2013) 5580–5599.

[34] A. Castegna, P. Scarcia, G. Agrimi, L. Palmieri, H. Rottensteiner, I. Spera, L. Germinario, F. Palmieri, Identification and functional characterization of a novel mitochondrial carrier for citrate and oxoglutarate in *Saccharomyces cerevisiae*, J. Biol. Chem. 285 (2010) 17359–17370.

[35] L. Ziegler, A. Terzulli, R. Gaur, R. McCarthy, D.J. Kosman, Functional characterization of the ferroxidase, permease high-affinity iron transport complex from *Candida albicans*, Mol. Microbiol. 81 (2011) 473–485.

[36] M.E. Marvin, R.P. Mason, A.M. Cashmore, The CaCTR1 gene is required for high-affinity iron uptake and is transcriptionally controlled by a copper-sensing transactivator encoded by CaMAC1, Microbiology 150 (2004) 2197–2208.

[37] R.A. Gaxiola, D.S. Yuan, R.D. Klausner, G.R. Fink, The yeast CLC chloride channel functions in cation homeostasis, Proc. Natl. Acad. Sci. 95 (1998) 4046–4050.

[38] M. Shakoury-Elizeh, O. Protchenko, A. Berger, J. Cox, K. Gable, T.M. Dunn, W.A. Prinz, M. Bard, C.C. Philpott, Metabolic response to iron deficiency in *Saccharomyces cerevisiae*, J. Biol. Chem. 285 (2010) 14823–14833.

[39] C.C. Philpott, S. Leidgens, A.G. Frey, Metabolic remodeling in iron-deficient fungi, Biochim. Biophys. Acta, Mol. Cell Res. 1823 (2012) 1509–1520.

[40] S. Ekici, S. Turkarslan, G. Pawlik, A. Dancis, N.S. Baliga, H.G. Koch, F. Daldal, Intracytoplasmic copper homeostasis controls cytochrome c oxidase production, mBio 5 (2014) e01055-13.

[41] C. Förster, P.M. Kane, Cytosolic $Ca^{2+}$ homeostasis is a constitutive function of the V-ATPase in *Saccharomyces cerevisiae*, J. Biol. Chem. 275 (2000) 38245–38253.

[42] E.M. Vasicek, E.L. Berkow, S.A. Flowers, K.S. Barker, P.D. Rogers, UPC2 is universally essential for azole antifungal resistance in *Candida albicans*, Eukaryot. Cell 13 (2014) 933–946.

[43] K. Dawson, W.M. Toone, N. Jones, C.R.M. Wilkinson, Loss of regulators of vacuolar ATPase function and ceramide synthesis results in multidrug sensitivity in *Schizosaccharomyces pombe*, Eukaryot. Cell 7 (2008) 926–937.

[44] D. Sanglard, F. Ischer, T. Parkinson, D. Falconer, J. Bille, *Candida albicans* mutations in the ergosterol biosynthetic pathway and resistance to several antifungal agents, Antimicrob. Agents Chemother. 47 (2003) 2404–2412.

[45] F. Abe, T. Hiraki, Mechanistic role of ergosterol in membrane rigidity and cycloheximide resistance in *Saccharomyces cerevisiae*, BBA Biomembr. 1788 (2009) 743–752.

[46] R.D. Cannon, E. Lamping, A.R. Holmes, K. Niimi, P.V. Baret, M.V. Keniya, K. Tanabe, M. Niimi, A. Goffeau, B.C. Monk, Efflux-mediated antifungal drug resistance, Clin. Microbiol. Rev. 22 (2009) 291–321.

[47] I. Ivnitski-Steele, A.R. Holmes, E. Lamping, B.C. Monk, R.D. Cannon, L.A. Sklar, Identification of Nile red as a fluorescent substrate of the *Candida albicans* ATP-binding cassette transporters Cdr1p and Cdr2p and the major facilitator superfamily transporter Mdr1p, Anal. Biochem. 394 (2009) 87–91.

[48] L. Chen, Y. Xu, C. Zhou, J. Zhao, C. Li, R. Wang, Overexpression of CDR1 and CDR2 genes plays an important role in fluconazole resistance in *Candida albicans* with G487T and T916C mutations, J. Int. Med. Res. 38 (2010) 536–545.

[49] S. Cheng, C.J. Clancy, K.T. Nguyen, W. Clapp, M.H. Nguyen, A *Candida albicans* petite mutant strain with uncoupled oxidative phosphorylation overexpresses MDR1 and has diminished susceptibility to fluconazole and voriconazole, Antimicrob. Agents Chemother. 51 (2007) 1855–1858.

[50] K. Nakamura, M. Niimi, K. Niimi, A.R. Holmes, J.E. Yates, A. Decottignies, B.C. Monk, A. Goffeau, R.D. Cannon, Functional expression of *Candida albicans* drug efflux pump Cdr1p in a *Saccharomyces cerevisiae* strain deficient in membrane transporters, Antimicrob. Agents Chemother. 45 (2001) 3366–3374.

[51] X. Jia, Y. Wang, Y. Jia, P. Gao, Y. Xu, L. Wang, Y. Cao, Y. Cao, L. Zhang, Y. Jiang, RTA2 is involved in calcineurin-mediated azole resistance and sphingoid long-chain base release in *Candida albicans*, Cell. Mol. Life Sci. 66 (2009) 122–134.

[52] K.-J. Dietz, N. Tavakoli, C. Kluge, T. Mimura, S. Sharma, G. Harris, A. Chardonnens, D. Golldack, Significance of the V-type ATPase for the adaptation to stressful growth conditions and its regulation on the molecular and biochemical level, J. Exp. Bot. 52 (2001) 1969–1980.

[53] Y. Jia, R.J. Tang, L. Wang, X. Zhang, Y. Wang, X.M. Jia, Y.Y. Jiang, Calcium-activated-calcineurin reduces the In vitro and In vivo sensitivity of fluconazole to *Candida albicans* via Rta2p, PLoS One 7 (2012) e48369.

[54] M. Craig, S. Lambert, S. Jourdan, E. Tenconi, S. Colson, M. Maciejewska, M. Ongena, J.F. Martin, G. van Wezel, S. Rigali, Unsuspected control of siderophore production by N-acetylglucosamine in *streptomycetes*, Environ. Microbiol. Rep. 4 (2012) 512–521.

[55] E.M. Michelle, G. Sergio, The vacuolar-type $H^+$-ATPase at a glance-more than a proton pump, J. Cell Sci. 127 (2014) 4987–4993.

[56] G.-H. Sun Wada, Y. Wada, Role of vacuolar-type proton ATPase in signal transduction, BBA Bioenerg. 1847 (2015) 1166–1172.

[57] K. Schumacher, D. Vafeados, M. McCarthy, H. Sze, T. Wilkins, J. Chory, The Arabidopsis det3 mutant reveals a central role for the vacuolar $H^+$-ATPase in plant growth and development, Gene. Dev. 13 (1999) 3259–3270.

[58] J. Hilty, A.G. Smulian, S.L. Newman, The *Histoplasma capsulatum* vacuolar ATPase is required for iron homeostasis, intracellular replication in macrophages and virulence in a murine model of histoplasmosis, Mol. Microbiol. 70 (2008) 127–139.

[59] C.C. Askwith, D. Silva, J. Kaplan, Molecular biology of iron acquisition in *Saccharomyces cerevisiae*, Mol. Microbiol. 20 (1996) 27–34.

[60] D.C. Radisky, W.B. Snyder, S.D. Emr, J. Kaplan, Characterization of VPS41, a gene required for vacuolar trafficking and high-affinity iron transport in yeast, Proc. Natl. Acad. Sci. 94 (1997) 5662–5666.

[61] U. Schlecht, S. Suresh, W.H. Xu, A.M. Aparicio, A. Chu, M.J. Proctor, R.W. Davis, C. Scharfe, R.P. St Onge, A functional screen for copper homeostasis genes identifies a pharmacologically tractable cellular system, BMC Genomics 15 (2014).

[62] Y. Ohya, N. Umemoto, I. Tanida, A. Ohta, H. Iida, Y. Anraku, Calcium-sensitive cls mutants of *Saccharomyces cerevisiae* showing a Pet-phenotype are ascribable to defects of vacuolar membrane H (+)-ATPase activity, J. Biol. Chem. 266 (1991) 13971–13977.

[63] Q.L. Yu, H. Wang, N. Xu, X.X. Cheng, Y.Z. Wang, B.A. Zhang, L.J. Xing, M.C. Li, Spf1 strongly influences calcium homeostasis, hyphal development, biofilm formation and virulence in *Candida albicans*, Microbiol-Sgm 158 (2012) 2272–2282.

[64] C.Y. Lan, G. Rodarte, L.A. Murillo, T. Jones, R.W. Davis, J. Dungan, G. Newport, N. Agabian, Regulatory networks affected by iron availability in *Candida albicans*, Mol. Microbiol. 53 (2004) 1451–1469.

[65] R.A. Fratti, P.H. Belanger, M.A. Ghannoum, J.E. Edwards, S.G. Filler, Endothelial cell injury caused by *Candida albicans* is dependent on iron, Infect. Immun. 66 (1998) 191–196.

[66] C.K. Mukhopadhyay, Z.K. Attieh, P.L. Fox, Role of ceruloplasmin in cellular iron uptake, Science 279 (1998) 714–717.

[67] K.M. Comerford, T.J. Wallace, J. Karhausen, N.A. Louis, M.C. Montalto, S.P. Colgan, Hypoxia-inducible factor-1-dependent regulation of the multidrug resistance (MDR1) gene, Cancer Res. 62 (2002) 3387–3394.

[68] H. Elicharova, H. Sychrova, Fluconazole affects the alkali-metal-cation homeostasis and susceptibility to cationic toxic compounds of *Candida glabrata*, Microbiology 160 (2014) 1705–1713.

[69] S.S. Gupta, V.-K. Ton, V. Beaudry, S. Rulli, K. Cunningham, R. Rao, Antifungal activity of amiodarone is mediated by disruption of calcium homeostasis, J. Biol. Chem. 278 (2003) 28831–28839.

[70] C.J. Hu, C. Bai, X.D. Zheng, Y.M. Wang, Y. Wang, Characterization and functional analysis of the siderophore-iron transporter CaArn1p in *Candida albicans*, J. Biol. Chem. 277 (2002) 30598–30605.

[71] M. Gerami-Nejad, J. Berman, C.A. Gale, Cassettes for PCR-mediated construction of green, yellow, and cyan fluorescent protein fusions in *Candida albicans*, Yeast 18 (2001) 859–864.